Quarterly Reviews of Biophysics **35**, 3 (2002), pp. 287–325. © 2002 Cambridge University Press
DOI: 10.1017/S0033583502003803 Printed in the United Kingdom

Biophysical basis of brain activity: implications for neuroimaging

Robert G. Shulman[1,2], Fahmeed Hyder[2,3,4] and Douglas L. Rothman[2,3,4]

Magnetic Resonance Center for Research in Metabolism and Physiology, Departments of [1] Molecular Biophysics and Biochemistry, [2] Diagnostic Radiology, [3] Biomedical Engineering, and [4] Section of Bioimaging Sciences, Yale University School of Medicine, New Haven, CT, USA

1. **Summary 288**
2. **Introduction 288**
3. **Relationship between neuroenergetics and neurotransmitter flux 294**
4. **A model of coupling between neuroenergetics and neurotransmission 296**
5. **Relationship between neuroenergetics and neural spiking frequency 297**
6. **Comparison with previous electrophysiological and fMRI measurements 298**
7. **Contributions of non-oxidative energetics to a primarily oxidative brain 299**
8. **Possible explanation for non-oxidative energetics contributions 300**
9. **A model of total neuronal activity to support cerebral function 302**
10. **Implications for interpretation of fMRI studies 305**
11. **The restless brain 306**
12. **Acknowledgements 310**
13. **Appendix A. CMR_{O_2} by ^{13}C-MRS 310**
14. **Appendix B. V_{cyc} and test of model 313**
15. **Appendix C. CMR_{O_2} by calibrated BOLD 316**
16. **Appendix D. Comparison of spiking activity of a neuronal ensemble with CMR_{O_2} 318**
17. **References 320**

Address for correspondence: Robert G. Shulman, C112 SHM, 333 Cedar Street, Yale University, New Haven, CT 06510, USA.
Tel.: (203) 785-6201; Fax: (203) 785-6205; E-mail: robert.shulman@yale.edu

https://doi.org/10.1017/S0033583502003803 Published online by Cambridge University Press

1. Summary

In vivo ^{13}C magnetic resonance spectroscopy (MRS) studies of the brain have quantitatively assessed rates of glutamate–glutamine cycle (V_{cyc}) and glucose oxidation ($CMR_{Glc(ox)}$) by detecting ^{13}C label turnover from glucose to glutamate and glutamine. Contrary to expectations from *in vitro* and *ex vivo* studies, the *in vivo* ^{13}C-MRS results demonstrate that glutamate recycling is a major metabolic pathway, inseparable from its actions of neurotransmission. Furthermore, both in the awake human and in the anesthetized rat brain, V_{cyc} and $CMR_{Glc(ox)}$ are stoichiometrically related, where more than two thirds of the energy from glucose oxidation supports events associated with glutamate neurotransmission. The high energy consumption of the brain measured at rest and its quantitative relation to neurotransmission reflects a sizeable activity level for the resting brain. The high activity of the non-stimulated brain, as measured by cerebral metabolic rate of oxygen use (CMR_{O_2}), establishes a new neurophysiological basis of cerebral function that leads to reinterpreting functional imaging data because the large baseline signal is commonly discarded in cognitive neuroscience paradigms. Changes in energy consumption (ΔCMR_{O_2}%) can also be obtained from magnetic resonance imaging (MRI) experiments, using the blood oxygen level-dependent (BOLD) image contrast, provided that all the separate parameters contributing to the functional MRI (fMRI) signal are measured. The BOLD-derived ΔCMR_{O_2}% when compared with alterations in neuronal spiking rate ($\Delta\nu$%) during sensory stimulation in the rat reveals a stoichiometric relationship, in good agreement with ^{13}C-MRS results. Hence fMRI when calibrated so as to provide ΔCMR_{O_2}% can provide high spatial resolution evaluation of neuronal activity. Our studies of quantitative measurements of changes in neuroenergetics and neurotransmission reveal that a stimulus does not provoke an arbitrary amount of activity in a localized region, rather a total level of activity is required where the increment is inversely related to the level of activity in the non-stimulated condition. These biophysical experiments have established relationships between energy consumption and neuronal activity that provide novel insights into the nature of brain function and the interpretation of fMRI data.

2. Introduction

The human brain comprising of only about 2% of the body mass accounts for approximately 20% of its total oxygen consumption (Sokoloff, 1991). The utilization of this large amount of energy and its relation to cerebral function forms a fascinating research narrative of the recent past. Coupled with the well established finding that glucose is the main, almost exclusive, carbon source for brain, it is expected and generally well accepted that glucose oxidation is the main cerebral energy-producing pathway. Modern studies of the relation between the delivery of this fuel to the brain by blood flow and its metabolism started with Roy & Sherrington (1890) who suggested that 'an automatic mechanism by which the blood supply of any part of the cerebral tissue is varied in accordance with the activity of the chemical changes which underlie the functional activation of that part'. This hypothesis framed the neurophysiological assumption that blood flow, energetics, and neuronal functions are tightly coupled. In the next decades, components of this assumption were studied separately.

https://doi.org/10.1017/S0033583502003803 Published online by Cambridge University Press

The early whole-brain studies of cerebral metabolic rates of glucose (CMR_{Glc}) and oxygen (CMR_{O_2}) consumption, estimated by arterio–venous differences in conjunction with cerebral blood flow (CBF) were measured by inhaled inert gases (for a review see Siesjo, 1978). These global results provoked the need to localize changes in these parameters induced by stimulation, and therefore, to infer regional changes in neuronal functions. Louis Sokoloff (National Institute of Health, Bethesda, MD, USA), pioneered autoradiographic methods for localized neuroimaging in animal models. An autoradiographic method (Sokoloff *et al*. 1977), infusing a radioactive glucose analog (^{14}C-2-deoxyglucose), was developed to measure localized changes in CMR_{Glc}. Another autoradiographic method (Sakurada *et al*. 1978), using an intravascular radioactive tracer ([^{14}C]iodoantipyrine), was used to measure localized changes in CBF. Both these techniques measured absolute values of CMR_{Glc} and CBF and these quantitative methods were major steps towards modern neuroimaging.

These techniques were applied to both awake and anesthetized animals (for a review see Sokoloff, 1981). The results from rats in non-stimulated conditions showed that CMR_{Glc} and CBF were regionally coupled, providing early support for part of the Roy & Sherrington (1890) suggestion (Mies *et al*. 1981a, b). A similar level of regional coupling was observed during stimulation. In many animal studies of stimulus-induced brain activation – including visual stimulation (Kennedy *et al*. 1976; des Rosiers *et al*. 1978), limb stimulation (Santori *et al*. 1986; Ueki *et al*. 1988), and whisker stimulation (Ginsberg *et al*. 1987; Kossut *et al*. 1988) – linearity between ΔCBF % and ΔCMR_{Glc} % was observed with stoichiometries close to unity. Although localized changes in CMR_{O_2} were not measured in these animal studies, the coupled localized increases in CBF and CMR_{Glc} during stimulation, considered together with globally averaged values of CMR_{Glc} and CMR_{O_2}, supported the belief that under *both* non-stimulated and stimulated conditions, energy was produced oxidatively (Kuschinsky *et al*. 1981; Dietrich *et al*. 1986). Therefore, a concept of neurovascular coupling was established from these autoradiographic studies, i.e. localized increases in energy, mainly from the oxidation of glucose, are linked to changes in blood flow and neuronal activity.

To extend these autoradiograhic methods (which required the animal to be sacrificed) for human studies, analogous schemes were developed for non-invasive measurements using positron emission tomography (PET). ^{19}F-fluoro-deoxyglucose was developed as a radioactive tracer to measure changes in CMR_{Glc} (Reivich *et al*. 1979) and CBF was measured by use of ^{15}O-water (Raichle *et al*. 1983). The ^{11}O-carbon monoxide tracer, which mimics the binding of oxygen to hemoglobin in red blood cells, was able to measure cerebral blood volume (CBV) changes (Phelps *et al*. 1979). An additional tracer (inhaled ^{15}O-oxygen) was developed (Raichle *et al*. 1979) to model unidirectional oxygen extraction from blood to brain (Krogh, 1919; Kreuzer, 1982). The combination of oxygen extraction, blood flow and volume methods enabled Raichle and colleagues to measure changes in CMR_{O_2} by PET (Mintun *et al*. 1984).

Quantitative functional studies of the human brain were initiated with PET approximately 15 years ago (for a review see Raichle, 1988). Since the 1990s magnetic resonance imaging (MRI) and spectroscopy (MRS) methods have played integral roles in functional brain studies (for a review see Shulman *et al*. 1993). PET functional studies were reinforced and extended by the discovery of functional MRI (fMRI) by Seiji Ogawa in 1990. This method, as originally proposed, depends on the effects of paramagnetic deoxyhemoglobin (in the blood) upon the nuclear magnetic resonance (NMR) transverse relaxation times of nearby water protons in the tissue (Ogawa *et al*. 1990). Since changes in the oxygen level in the blood can

https://doi.org/10.1017/S0033583502003803 Published online by Cambridge University Press

affect the fraction of hemoglobin in the deoxygenated state, the image contrast was termed as blood oxygenation level dependent (BOLD). The BOLD fMRI method has experimental advantages over the PET method (i.e. better contrast-to-noise ratio as well as higher spatial and temporal resolutions). Furthermore fMRI is readily measured by slight adaptation of clinical MRI scanners, which while expensive to purchase, are generally available in most modest clinical settings. Its non-invasive nature and the fact that it does not require radioactive tracers (which are necessary for PET experiments) have made fMRI the method of choice in neurobiological studies (for a review see Ogawa *et al*. 1998). After the initial demonstration of the BOLD method in the human brain (Bandettini *et al*. 1992; Blamire *et al*. 1992; Kwong *et al*. 1992; Ogawa *et al*. 1992), the cognitive neuroscience community immediately embraced the method.

Functional imaging methods can measure neurophysiological parameters separately, e.g. specific PET methods can determine CBF, CMR_{Glc}, or CMR_{O_2}. On the other hand, in the popular fMRI measurements the signal changes ($\Delta S\,\%$) depend upon ΔCBF % and ΔCMR_{O_2} % with a small contribution from ΔCBV % (for a review see Ugurbil *et al*. 2000). Because of its dependence upon several independent variables, quantitative interpretation of fMRI measurements has required sustained experimental research over the past decade. The usual fMRI experiments intend to localize sensory or psychological cerebral activities. However from a biophysical perspective the goal of fMRI studies is to derive the fundamental neuroenergetic parameter (i.e. CMR_{O_2}) from BOLD experimental results. This is accomplished by combining several independent MRI measurements (e.g. CBF and CBV) with the BOLD signal. These parameters when used to interpret BOLD data can derive values of ΔCMR_{O_2} % (for a review see Hyder *et al*. 2001), and thereby connect fMRI results with the developing body of information that relates CMR_{O_2} to neuronal activity (for a review see Shulman *et al*. 1999). In this paper we review this interpretation of BOLD in conjunction with other NMR methods for determining CMR_{O_2}.

The most established and quantitative relation between CMR_{O_2} and neuronal activity has come from *in vivo* ^{13}C-MRS studies in rats and humans (for reviews see Rothman *et al*. 1999, 2002). Since the resonance frequency of an NMR observable nucleus (e.g. ^{1}H, ^{13}C, ^{31}P, ^{15}N) depends on its chemical environment within the molecule, MRS can be used to detect biomolecules (in addition to water) *in vivo*. While ^{1}H-MRS is commonly used for measuring metabolite concentrations *in vivo* [e.g. aspartate, γ-amino butyric acid (GABA), glucose, glutamate, glutamine, and lactate], ^{13}C-MRS provides a unique window to cerebral metabolism. The non-radioactive, stable, ^{13}C isotope has a natural abundance of 1·1 % so that after the infusion of ^{13}C enriched substrates MRS can be used to measure the rates of isotopic incorporation into brain metabolites.

The ^{13}C brain MRS experiments started in the 1980s with direct detection of the ^{13}C flow from glucose to the pools of glutamate in the rat brain. Rates of ^{13}C label flow into glutamate were shown to be convertible to the tricarboxylic acid (TCA) cycle flux (V_{TCA}), which allows glucose oxidation ($CMR_{Glc(ox)}$) and oxygen consumption (CMR_{O_2}) rates to be quantitatively determined (see Appendix A). Values of $CMR_{Glc(ox)}$ and CMR_{O_2} in the non-stimulated brain obtained by ^{13}C-MRS agreed with previous measurements of CMR_{Glc} and CMR_{O_2} by arterio-venous difference, autoradiography, and PET methods (Mason *et al*. 1992, 1995; Hyder *et al*. 1996–2000). Direct ^{13}C-MRS (Behar *et al*. 1986) allowed for approximate localization of the signal in the cerebral cortex (typically $\sim$ 300 μl in rat brain). A proton observed carbon edit (POCE) method for indirect ^{13}C detection (Rothman *et al*. 1985) took advantage of ^{1}H

https://doi.org/10.1017/S0033583502003803 Published online by Cambridge University Press

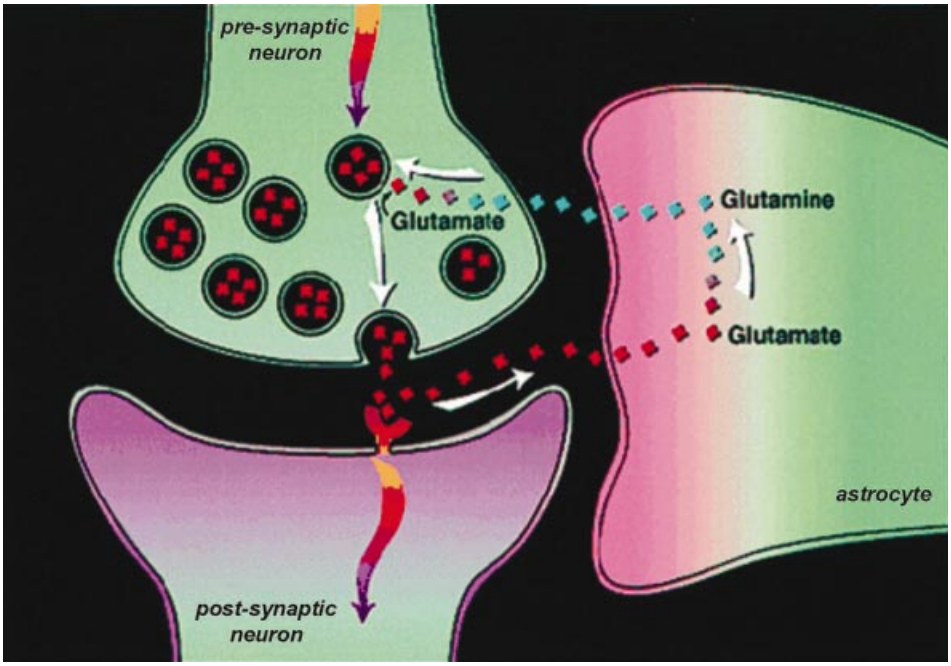


Fig. 1. A model of glutamate–glutamine neurotransmitter cycling between neurons and astrocytes (for a review see Magistretti *et al*. 1999). The rate of glutamate-to-glutamine cycle (V_{cyc}) has been quantitated by ^{13}C-MRS (for a review see Rothman *et al*. 1999). Action potentials or spikes (shown by curved arrows) reach the pre-synaptic terminal to initiate the release of vesicular glutamate into the synaptic cleft. This activates the glutamate receptors in the postsynaptic neuron, which is a step required in the propagation of spiking activity to the adjacent neuron (in an all-or-none manner). The extracellular glutamate is removed rapidly by Na^+-coupled transport into astrocytes, where it is converted into glutamine. The synthesized glutamine then passively diffuses back to the neuron, and after re-conversion to glutamate, is repackaged into vesicles. (Modified from Shulman & Rothman, 1998.)

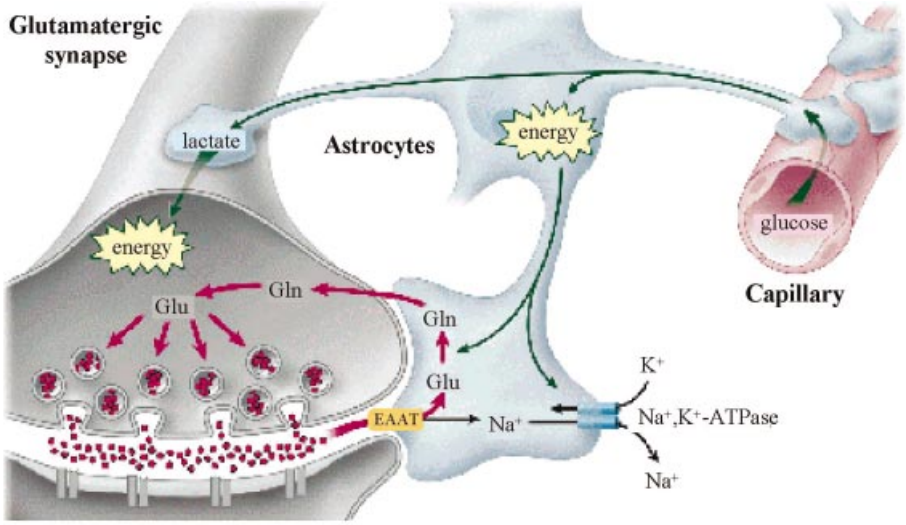
sensitivity to improve the spatial resolution several fold (typically $\sim$ 50 μl in rat brain). The most advanced applications of POCE can now obtain the ^{13}C-labeled glutamate signal from $\sim$ 8 μl voxels in rat brain (Hyder *et al*. 1999).

Improved NMR equipment performance subsequently allowed the ^{13}C-labeled glutamine signal to be detected and quantified over time of ^{13}C label incorporation (Gruetter *et al*. 1994). Just as the ^{13}C label flow from glucose to glutamate determined important neurophysiological parameters ($CMR_{Glc(ox)}$ and CMR_{O_2}; see Appendix A), analogously the subsequent ^{13}C label flow into glutamine allowed the glutamate neurotransmitter cycling through astrocytic glutamine (V_{cyc}; see Appendix B) to be determined in the rat (Sibson *et al*. 1997). These *in vivo* ^{13}C-MRS data provided support for a model of glutamate neurotransmitter cycling (Fig. 1): neuronal glutamate release and astrocytic clearance or uptake for conversion to glutamine, followed by glutamine transport back to neurons and final re-conversion to glutamate for vesicular packaging.

The model in Fig. 1, previously proposed by Berl *et al*. (1970) and van den Berg & Garfinkel (1971), was extended by Pellerin & Magistretti (1994) who proposed a quantitative coupling between glutamate neurotransmitter flux and energy consumption from *in vitro* cellular results as shown in Fig. 2. ^{13}C-MRS was used to test this proposal by simultaneous

https://doi.org/10.1017/S0033583502003803 Published online by Cambridge University Press

(*a*)



(*b*)

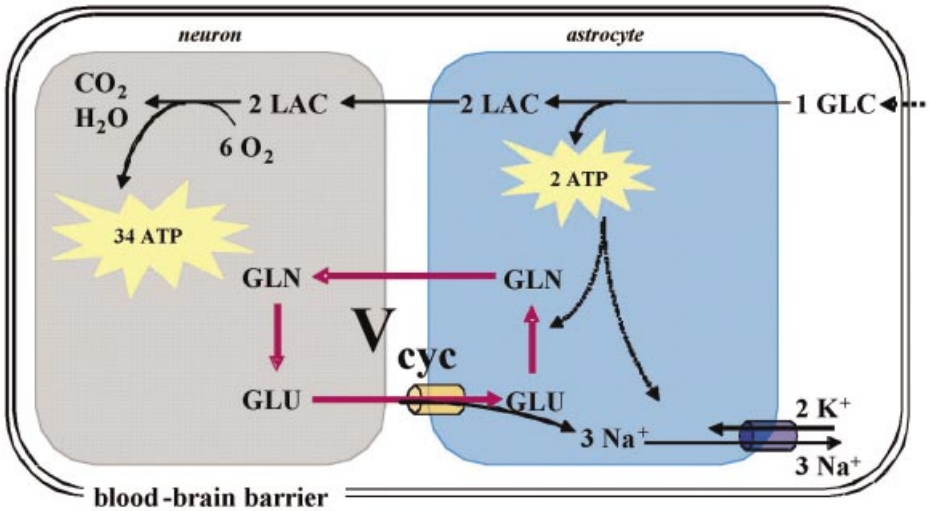


Fig. 2. A model of stoichiometric coupling between the rates of glutamate–glutamine neurotransmitter cycling (V_{cyc}) and glucose oxidation ($CMR_{Glc(ox)}$) (for a review see Magistretti *et al.* 1999). (*a*) Cytological association between capillaries, astrocytes, and neurons in the mammalian brain provide the framework for the century-old hypothesis of neurovascular coupling (Roy & Sherrington, 1890) which suggests that local neuronal activity is coupled with glucose utilization and blood flow. (*b*) Energy requiring processes associated with neuronal activity maintain resting cell membrane potential. The active Na^+–K^+ pump utilizes energy (i.e. ATP) to restore equilibrium Na^+ and K^+ concentrations in extracellular and intracellular compartments. The measured stoichiometry in Fig. 3 and Eq. (1) is consistent with the use of 2 ATP molecules in the asctrocyte. The remaining energy (~ 80 %) use in the neuron is connected with events associated with the recycling glutamate. Abbreviations: V_{cyc}, rate of glutamate neurotransmitter cycle; GLC, glucose; LAC, lactate; GLU, glutamate; and GLN, glutamine. (Modified from Magistretti *et al.* 1999.)

https://doi.org/10.1017/S0033583502003803 Published online by Cambridge University Press

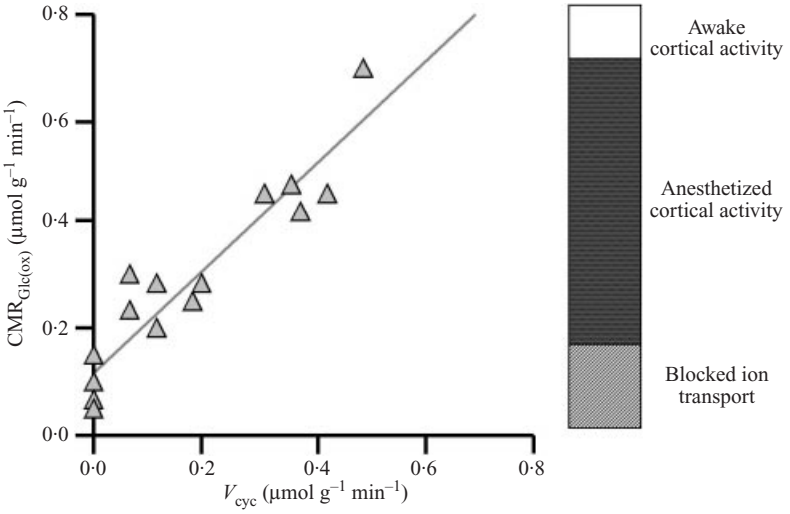


Fig. 3. Experimental results of V_{cyc} and $CMR_{Glc(ox)}$ from ^{13}C-MRS experiments at 7 T (Sibson *et al.* 1998) where rats were moderately anesthetized (with morphine and α-chloralose) to isoectric conditions (high-dose pentobarbital). The best-fit line is given by Eq. (1) (in units of μmol g^{-1} min^{-1}), which suggests that each mole of neurotransmitter glutamate cycling requires the oxidation of one mole of glucose. The awake, resting state has $CMR_{Glc(ox)}$ of approximately 0·8 μmol g^{-1} min^{-1}, which means that under this condition ~ 80% of the resting energy consumption is dedicated to events associated with V_{cyc}. (Modified from Sibson *et al.* 1998.)

measurements of V_{cyc} and $CMR_{Glc(ox)}$ (Sibson *et al.* 1998). The results shown in Fig. 3 agreed well with the expectations of the model in Fig. 2. The efficient use of neuroenergetics for neurotransmission, as suggested by the coupling between $CMR_{Glc(ox)}$ (or CMR_{O_2}) and V_{cyc} (Fig. 3), has been supported and extended by recent experiments (Fig. 4) in our laboratory (Smith *et al.* 2002). In this recent study, CMR_{O_2} derived from calibrated BOLD (see Appendix C) was shown to be coupled to the 'gold standard' of neuronal activity, i.e. the neuronal spiking frequency (ν) as measured by extracellular microelectrodes in the rat brain (see Appendix D).

In summary, our recent results show quantitative relationships between CMR_{O_2} and two separate steady state measurements of neurotransmission, i.e. glutamate neurotransmitter flux (V_{cyc}; Sibson *et al.* 1998; see Fig. 3) and neuronal spiking frequency (ν; Smith *et al.* 2002; see Fig. 4). Therefore we propose that changes in CMR_{O_2} provide a direct and non-invasive way of mapping neuronal activity in the intact brain. To this end, two different NMR methods for determining CMR_{O_2} have been developed in our laboratory: one from ^{13}C-MRS (see Appendix A) and the other from calibrated BOLD (see Appendix C). Absolute CMR_{O_2} values measured by ^{13}C-MRS have been validated by comparison with values obtained by other methods (Mason *et al.* 1992, 1995; Hyder *et al.* 1996–2000), whereas changes in CMR_{O_2} calculated from BOLD have been confirmed by comparisons with direct measurements from ^{13}C-MRS (Kida *et al.* 1999, 2000; Hyder *et al.* 2001). These combined results now provide a biophysical basis for BOLD fMRI signal in terms of neurotransmission and neuroenergetics. In this review, we first summarize our major NMR findings in the cerebral cortex (Figs. 3 and 4) which demonstrate that neurotransmission (i.e. work done) is directly coupled with neuroenergetics (i.e. energy consumed). We then discuss the implications of these results for the model proposed in Fig. 2 and demonstrate that our results are consistent with other

https://doi.org/10.1017/S0033583502003803 Published online by Cambridge University Press

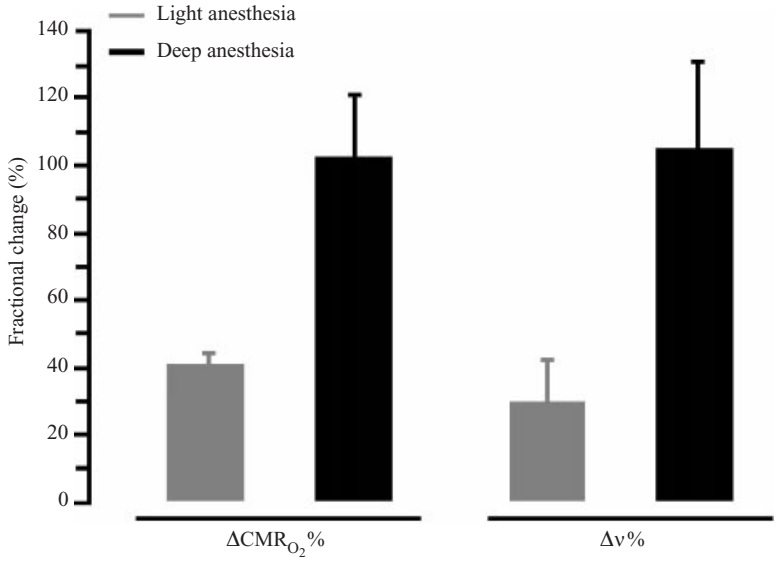


Fig. 4. Relationship between energy metabolism (ΔCMR_{O_2}%) and spiking frequency ($\Delta\nu$%) of a neuronal ensemble from calibrated fMRI (at 7 T) and concurrent electrophysiology experiments, respectively where rats were anesthetized with α-chloralose (see Appendix D). The bars represent the incremental stimulation-induced changes in CMR_{O_2} and ν from light (gray) and deep (black) anesthesia conditions (in the same rats for each method). The non-stimulated condition in deep anesthesia level was lowered by $\sim 30\%$ from the non-stimulated condition in light anesthesia level due to higher dosage of α-chloralose. The incremental change upon stimulation from deep anesthesia was larger. The ΔCMR_{O_2}% values were obtained from a total of 24 voxels (from all rats; $n = 6$) placed over the forelimb region (other activated voxels were not analyzed). The $\Delta\nu$% values were obtained from extracellular recordings of a total of 72 neurons in layer 4 of the forelimb region (from all rats; $n = 36$). The $\sim 1:1$ relation between ΔCMR_{O_2}% and $\Delta\nu$% agrees with results in Fig. 3. (Modified from Smith *et al.* 2002.)

measurements. On this basis we present an empirical, neurophysiological model of brain function that proposes a re-interpretation of functional imaging experiments designed to understand cerebral function.

3. Relationship between neuroenergetics and neurotransmitter flux

In early ^{13}C-MRS brain measurements the ^{13}C flow from [1-^{13}C]glucose to [4-^{13}C]glutamate was used to determine V_{TCA} from which both $CMR_{Glc(ox)}$ and CMR_{O_2} could be determined (for a review see Shulman *et al.* 1993). Details of the determination of these fluxes and the metabolic model describing the pathways are shown in Appendix A. Briefly, the infusion of [1-^{13}C]glucose lead to ^{13}C flow down the glycolytic pathway to pyruvate from which the label enters the TCA cycle, and subsequently flows through the small α-ketoglutarate pool (in μM range). The small α-ketoglutarate rapidly exchanges rapidly with the large glutamate pool (in mM range) so that the kinetics of ^{13}C label appearance depends upon the turnover of the combined pool, i.e. mainly glutamate. Thus V_{TCA} can be determined by the kinetic equations of ^{13}C label flow shown in Appendix A. The best-fit of the metabolic model to the near exponential rise of C4-glutamate ^{13}C fractional enrichment during steady state [1-^{13}C]glucose infusion allowed V_{TCA} to be calculated. Values of $CMR_{Glc(ox)}$ and CMR_{O_2} in the non-stimulated brain obtained by this approach agreed with previous measurements (Mason *et al.*

https://doi.org/10.1017/S0033583502003803 Published online by Cambridge University Press

1992, 1995; Hyder *et al*. 1996–2000), so that by the mid-1990s this *in vivo* ^{13}C-MRS method of measuring CMR_{O_2}, and therefore energy consumption, was well established.

At that time, due to technical improvements, it became possible to measure in the human brain *in vivo* the ^{13}C label flow into glutamine from glutamate (Gruetter *et al*. 1994), where a high rate of glutamine synthesis was measured (Mason *et al*. 1995). Glutamine is an intermediate in the proposed cycling of glutamate. Thus the ability to follow in time the ^{13}C label flow into glutamate and subsequently into glutamine by ^{13}C-MRS *in vivo* opened glutamate neurotransmitter cycling to quantitation. The glutamate neurotransmitter cycle (Fig. 1) was originally proposed by Berl *et al*. (1970) and van den Berg & Garfinkel (1971) from ^{14}C and ^{15}N studies of rat brains in the early 1970s. Additional evidence arose from enzyme and vesicle localization as well as isolated cell studies in the late 1980s and 1990s (for reviews see Torgner & Kvamme, 1990; Tsacopoulos & Magistretti, 1996). However the importance of this pathway *in vivo* was not known because of conflicting evidence from studies of brain slices (Badar-Goffer *et al*. 1990) and other *in vitro* preparations (Peng *et al*. 1993) which suggested that the rate of glutamine synthesis is low. In this glutamate neurotransmitter cycle model (Fig. 1), the action potential initiates the pre-synaptic release of vesicularized glutamate into the synaptic cleft. Once released it diffuses across the gap until it is recognized by glutamate receptors on the postsynaptic surface. There it triggers the subsequent postsynaptic potential changes. The majority of released glutamate is not retaken up by the pre-synaptic terminal but instead diffuses through the membranes of the surrounding astrocyte into which it is co-transported with Na^+ (for a review see Anderson & Swanson, 2000). The astrocytic enzyme glutamine synthetase then converts glutamate to glutamine consuming one ATP and one ammonia. Glutamine is transported across the astrocytic membrane, through the intracellular space, into the neuron, where the enzyme glutaminase reconverts it to glutamate. The glutamate is repackaged into vesicles where it is once again ready to restart the cycle. The first identification of both glutamate *and* glutamine turnover by ^{13}C-MRS was in the human brain at the rather low field of 2·1 T (Gruetter *et al*. 1994). As higher external fields of 4 and 7 T are becoming available spectral resolution and sensitivity have both improved.

Soon after these first experiments on human subjects, the easily manipulated rat model was exploited to expand the understanding of the interactions of the different rates *in vivo* (for a review see Rothman *et al*. 1999). The experimental results from the animal studies provided additional support for design and interpretation of subsequent human experiments (Gruetter *et al*. 1998; Shen *et al*. 1999; Lebon *et al*. 2002). The glutamate neurotransmitter cycle model (Fig. 1) suggests that the ^{13}C label flow into glutamine comes through a glutamate precursor so that interpreting the observed labeling of glutamine on this basis would allow the determination of the rate of glutamate neurotransmitter release, which is a consequence of pre-synaptic firing and its recycling through the astrocyte. The major interpretation of our ^{13}C-MRS results in regards to this model is that a large majority of the glutamate to glutamine flux ($\sim 80\,\%$) is from the pathway schematized in Fig. 1. For clarity of this discussion thus far, we have omitted possible uncertainties, alternatives, and/or approximations, which are discussed in detail in Appendix B. The maximum impact of these factors on the major interpretation of our ^{13}C-MRS results would be on the order of $\sim 10\,\%$ (for a review see Rothman *et al*. 1999). As data have accumulated it has become clear that this model is valid in rat and human brains, and more importantly the glutamate to glutamine flux is similar in magnitude to the glucose oxidation rate in both species (Sibson *et al*. 1997; Shen *et al*. 1999).

https://doi.org/10.1017/S0033583502003803 Published online by Cambridge University Press

The relative rates of glucose oxidation ($CMR_{Glu(ox)}$) and glutamate cycling (V_{cyc}) were measured over a wide range of brain activity in the rat (Sibson *et al*. 1998): deeply anesthetized conditions (pentobarbital), moderate depth of anesthesia (α-chloralose), and lightly anesthetized conditions (morphine). Simultaneous measurements of the ^{13}C flow into glutamate and of the subsequent flow into glutamine were converted into $CMR_{Glu(ox)}$ and V_{cyc}, respectively. Figure 3 and Eq. (1) summarize the results

$$CMR_{Glu(ox)} = V_{cyc} + 0{\cdot}1, \quad (1)$$

in units of $\mu mol\ g^{-1}\ min^{-1}$. The results are significant in several respects. First, a quantitative relationship between neurotransmission (i.e. neurotransmitter flux) and neuroenergetics (i.e. glucose oxidation) has been established. Secondly, at the intercept of Fig. 3 as V_{cyc} approaches zero, which corresponds to isoelectric conditions (i.e. no neuronal firing) achieved by deep pentobarbital anesthesia, $CMR_{Glu(ox)}$ falls to $\sim 0{\cdot}1\ \mu mol\ g^{-1}\ min^{-1}$ which is $\sim 15\%$ of the value at non-stimulated awake condition ($\sim 0{\cdot}8\ \mu mol\ g^{-1}\ min^{-1}$). Since only $\sim 15\%$ of the basal non-stimulated energy consumption is needed to support the brain in the absence of neuronal firing, in the non-stimulated awake condition $\sim 85\%$ of the energy supports events associated with neurotransmission. This high level of brain activity in the absence of specific stimulations is a novel neuroscientific finding from these experiments which, as discussed below, has required fundamental re-evaluation of neuroimaging data. Thirdly, the slope of the $CMR_{Glu(ox)}$ and V_{cyc} curve is ~ 1. For clarity of presentation of data in Fig. 3, the measured value of V_{TCA} has been converted into $CMR_{Glu(ox)}$ assuming stoichiometries of the idealized brain metabolism where the only carbon source is glucose and it is all oxidized (see Appendix A). The slope of unity (within the accuracy of this simplification) means that for every additional glucose molecule oxidized one glutamate is released as a neurotransmitter and cycled through glutamine. This stoichiometry allows changes in neurotransmitter flux (which can only be measured directly in this type of a ^{13}C-MRS experiment) to be determined from measured changes in oxygen consumption. These results are in accord with and provide support for the *in vivo* activity of molecular and cellular models proposed by *in vitro* studies (for reviews see Pellerin & Magistretti, 1994; Tsacopoulos & Magistretti, 1996) which link energy consumption to neuronal firing. The model framework allows for different pathways to be tested and validated *in vivo*. Current studies in our laboratory suggest that there are small but measurable contributions to neuroenergetics from non-glutamatergic neurons (e.g. GABAergic) (Rothman *et al*. 2002).

4. A model of coupling between neuroenergetics and neurotransmission

In studies of glial cells in suspension, Pellerin & Magistretti (1994) observed a coupling between glutamate uptake and lactate production. The relationship of 2 lactates per glutamate uptake led them to suggest a 1:1 stoichiometry between glucose breakdown (metabolized to lactate in the astrocyte) and glutamate uptake (co-transported with Na^+ into the astrocyte). This observation was subsequently supported by ^{13}C-MRS evaluation of glutamate recycling and glucose oxidation (Fig. 3). The Pellerin & Magistretti (1994) model was thus extended with the *in vivo* ^{13}C-MRS data to comprehensively cover the pathways and reactions that would be required *in vivo* (Fig. 2).

As shown in Fig. 2, the concept of localized cellular energetics and the coupling between the rates of ATP production and consumption in the astrocyte agreed with the measured *in*

https://doi.org/10.1017/S0033583502003803 Published online by Cambridge University Press

vivo stoichiometries of glucose consumed (oxidatively) per glutamate cycled measured by ^{13}C-MRS. Glycolysis in glia would produce 2 ATP equivalents from 1 glucose breakdown, where 1 ATP would serve to restore the Na^+/K^+ gradient and the other would energize the glutamine synthetase formation of glutamine from glutamate and ammonia. Therefore at steady state the stoichiometries of glycolysis agreed with the glial need for two ATP equivalents per glutamate. The glial lactate would diffuse to the neurons where, proceeding via pyruvate, it would be oxidized to generate the larger fraction of the ATP (see Appendix A).

While the stoichiometries of the model in Fig. 2 have been generally accepted because they are based on direct ^{13}C-MRS measurements which have been tested rather thoroughly (see Appendix B), the proposal of lactate as the sole glial–neuronal connection lacks direct experimental support. The possibilities remain that oxidative glial energy (which is neglected in the model) could provide some of the energy for glutamine synthesis and restore ion gradients, and some fraction of neuronal fuel could come directly from glucose because of the availability of glucose transporters as well as the presence of glycolytic enzymes in neurons. While these proposals and replies to them have been reviewed lately (Magistretti *et al*. 1999; Rothman *et al*. 1999), the exclusiveness of lactate as a neuronal–glial bridge remains uncertain. Some aspects for the role of lactate are discussed below. The strongest reinforcement of the model (Fig. 2) and the coupling between $CMR_{Glc(ox)}$ and V_{cyc} (Fig. 3) comes from recent experiments relating energy consumption (CMR_{O_2}) to the spiking frequency of neurons (ν), which is discussed immediately below.

5. Relationship between neuroenergetics and neural spiking frequency

The frequency of neuronal spiking measured by extracellular recordings is considered to be the 'gold standard' of brain activity (Kandel *et al*. 1991). The extracellular recordings (with single or multiple microelectrodes) comprise the activity of a small group of neurons near the electrode tip (< 1 μm). Although spiking is only one of a variety of electrical signals that are recorded extracellularly, action potentials are more easily identifiable signals *in vivo* because they are short-lived, have relatively high signal-to-noise ratio, and their different spike shapes can be assigned to different neurons in an ensemble (Kandel *et al*. 1991; Gray *et al*. 1995; Chapin & Nicolelis, 1999; Zouridakis & Tam, 2000).

In a recent study (Smith *et al*. 2002; Appendix D), we measured the energy consumption (CMR_{O_2}) and correlated it with spiking frequency of a neuronal ensemble (ν) in a localized region of the rat brain (Fig. 4). This study provided an additional test for the coupling between $CMR_{Glc(ox)}$ and V_{cyc} suggested by ^{13}C-MRS experiments (Fig. 3). In this study, the energy metabolism was based on the values of ΔCMR_{O_2}% from calibrated BOLD, as described previously (Kida *et al*. 1999, 2000; Hyder *et al*. 2001) and reviewed in Appendix C. Hence, it was possible to derive a validated value of ΔCMR_{O_2}% with the high signal-to-noise ratio and spatial resolution of fMRI. As described in Appendix D, the extracellular electrodes identified specific spikes by their electrical properties (as recognized by spike amplitude, duration, latency, etc.) and then the spiking frequencies under the different conditions were measured. The spiking activities from a total of 72 neurons were identified and followed for four conditions in the same rat: two levels of α-chloralose anesthesia, with and without forepaw stimulation. To accurately determine absolute firing rates more experiments will

https://doi.org/10.1017/S0033583502003803 Published online by Cambridge University Press

have to be conducted so that the statistics would more accurately represent firing rates of the entire neuronal population.

In the α-chloralose-anesthetized rat during forepaw stimulation $\Delta\nu\%$ was correlated with $\Delta CMR_{O_2}\%$ over a wide range of activity (Fig. 4), with the result that

$$\Delta CMR_{O_2}\% \approx \Delta\nu\%. \quad (2)$$

The relationship of Eq. (2) was derived from forepaw stimulation from either of the two depths of anesthesia as well as from the difference between the two non-stimulated baseline conditions at different depths of anesthesia. These results extend reports by Sokoloff (1993) and co-workers that glucose utilization in peripheral neurons increases proportionately with stimulation frequency. However this is the first quantitative study to show the relationship between electrical activity of neurons and energy metabolism in the intact mammalian brain. By combining Eqs. (1) and (2) we obtain

$$\Delta CMR_{O_2}\% \approx \Delta\nu\% \approx \Delta V_{cyc}\%. \quad (3)$$

Equation (3) suggests that $\Delta CMR_{O_2}\%$, the incremental energy consumption, is thereby related to both aspects of neurotransmission (i.e. neurotransmitter flux and neuronal spiking rate) and establishes a quantitative relation between three important biophysical parameters: the flux of the glutamate neurotransmitter release and its cycling back to neurons (V_{cyc}) as well as the relative spiking frequency of an ensemble of glutamatergic neurons (ν) are both directly coupled to the energy consumption (CMR_{O_2}). Since the $\Delta CMR_{O_2}\%$ was derived from calibrated BOLD in these combined fMRI and electrophysiological studies (Smith *et al.* 2002), the results in Eq. (3) also provide a biophysical basis of fMRI. Merely phenomenological relationships have been reported by comparison of the spatial and temporal profiles of the electrical and BOLD signals (see below). In contrast, our results (Fig. 4) have established a biophysical relationship between fMRI and electrical signals because the values of $\Delta CMR_{O_2}\%$ (from calibrated BOLD) are directly correlated with $\Delta\nu\%$ (from extracellular recordings).

6. Comparison with previous electrophysiological and fMRI measurements

Combined fMRI and electrophysiology studies in rodents (Yang *et al.* 1997; Brinker *et al.* 1999; Ogawa *et al.* 2000) and in primates (Rees *et al.* 2000; Logothetis *et al.* 2001) have shown in different ways that the stimulus-induced electrical activity of neurons (as measured by electroencephalogram, local field potentials, or spiking activity) is spatially co-localized with the BOLD response. However the existence of a quantitative relationship has been controversial.

Rees *et al.* (2000) suggested that a $\sim 1\%$ change in the BOLD signal (at 1·5 T in humans) corresponds to ~ 9 Hz change in the spiking rate per neuron in region V5 (of primate) visual cortex. This proportionality between $\Delta\nu\%$ and $\Delta S\%$ for the visual cortex drawn from interspecies data was not consistent with observations from other brain regions and/or data from other laboratories (Heeger *et al.* 2000). These large variations in the proportionality between $\Delta\nu\%$ and $\Delta S\%$ may largely reflect variations in the biophysical determinants of BOLD contrast (Ogawa *et al.* 1998; Ugurbil *et al.* 2000), rather than fundamental differences in the coupling between energy metabolism and electrical activity. Since differences in cellular

https://doi.org/10.1017/S0033583502003803 Published online by Cambridge University Press

and vascular anatomy across species (Braitenberg & Schuz, 1991) were not considered at all, direct and quantitative cross species comparison of spiking rates was not fully justified since it is unlikely that firing rates across species are preserved (Kristan & Shaw, 1997).

Logothetis *et al*. (2001) concluded that changes in the BOLD signal (at 4·7 T in primates) represent the neuronal input because they observed a high correlation between time-courses of BOLD signal and local field potentials. It may be argued that the time-courses of local field potentials reflect the neuronal input because they represent the weighted sum of the changing membrane potentials in dendrites and soma, which result from spiking of neighboring neurons (Kandel *et al*. 1991). However, since most of the synapses in the cerebral cortex are local (Braitenberg & Schuz, 1991), the input and output signals in a neuronal ensemble are not entirely distinguishable. Thus it is inappropriate to link the fMRI signal to either the input or output of the system.

In contrast, the relationship found in our recent study between changes in CMR_{O_2} and ν (Smith *et al*. 2002) has the advantage over previous studies of not depending upon any complex biophysical or technical fMRI parameters (e.g. field strength or pulse sequence). Nor does it depend upon statistical determinants of BOLD contrast. These factors are effectively normalized by the BOLD calibration and validation procedure (Kida *et al*. 1999, 2000; Hyder *et al*. 2001) and by using the same stimulation for both basal conditions (in the same rats). In our study, the BOLD signal changes yield values of ΔCMR_{O_2}% which provide a quantitative relationship with $\Delta\nu$%, the rate of neuronal spiking activity (Fig. 4). These results provide a biophysical relation between the neuroimaging signal and a basic measurement of neuronal activity, which agrees with the relationship between ΔCMR_{O_2}% and ΔV_{cyc}% obtained from ^{13}C-MRS studies (Fig. 3). The main consequence of these findings is that the BOLD signal when calibrated to obtain values of CMR_{O_2} can be used to map pyramidal cell electrical activity in the somatosensory cortex.

7. Contributions of non-oxidative energetics to a primarily oxidative brain

Our recent results show a direct correlation between CMR_{O_2} and two separate measurements of neurotransmission, i.e. glutamate neurotransmitter flux (V_{cyc}; Sibson *et al*. 1998) and neuronal spiking frequency (ν; Smith *et al*. 2002) at steady state. Over a wide range of neuronal activity, whether the activity is increased or decreased from a particular basal level, oxidation of glucose provides the major source of energy for neurotransmission. This constant relationship between oxidative neuroenergetics and glutamatergic neurotransmission appears to be inconsistent with certain findings from PET studies of a greater increase in ΔCMR_{Glc}% than ΔCMR_{O_2}% during stimulation (Fox & Raichle, 1986; Fox *et al*. 1988). The functional studies in humans measuring changes in CMR_{Glc}, CMR_{O_2}, and CBF by PET reported $\sim$ 50% increase in CMR_{Glc} and CBF *versus* $\sim$ 5% increase in CMR_{O_2} upon sensory stimulation. Because this finding represented a departure from the generally accepted idea that the brain was supported entirely by glucose oxidation (Siesjo, 1978), the authors proposed that stimulated activity was supported by anaerobic glycolysis. This posed the question as to whether mechanisms of energy supply were different above and below the non-stimulated awake level of activity.

Although subsequent PET and NMR experiments did not find such extreme inequality, they did qualitatively support the observation of inequality between ΔCMR_{Glc}% and

https://doi.org/10.1017/S0033583502003803 Published online by Cambridge University Press

ΔCMR_{O_2}%. More than a dozen reports of human sensory stimulation studies averaged to $\Delta CMR_{Glc}\% \approx 30\%$ and $\Delta CMR_{O_2}\% \approx 20\%$ (for a review see Shulman *et al*. 2001a), where the ratio of $(\Delta CMR_{O_2}\%)/(\Delta CMR_{Glc}\%)$ is in good agreement with animal sensory stimulation studies (for a review see Hyder *et al*. 2000). It is noteworthy that glucose oxidation contributes the majority of ATP even in the extreme uncoupled case of $\Delta CMR_{Glc}\% \approx 50\%$ and $\Delta CMR_{O_2}\% \approx 5\%$, and it completely dominates ATP production in the more moderately uncoupled case of $\Delta CMR_{Glc}\% \approx 30\%$ and $\Delta CMR_{O_2}\% \approx 20\%$. A recent report from a temporally resolved PET study of CMR_{O_2} changes during functional activation (Mintun *et al*. 2002) showed that the greatest mismatch between aerobic and anaerobic glucose breakdown occurred immediately following stimulation onset, whereas during steady-state stimulation the mismatch is significantly reduced. While the established finding that under non-stimulated conditions glucose oxidation is the main energy producing pathway, the small but definite contributions from non-oxidative sources (where lactate is the end product) particularly under stimulated conditions cannot be ignored.

Whereas modern brain-imaging methods have allowed the differences between $\Delta CMR_{Glc}\%$ and $\Delta CMR_{O_2}\%$ to be determined during sensory stimulation, greater discrepancies have long been known during seizures. Typical incremental values during bicuculline-induced seizures in the anesthetized rat are $\Delta CMR_{Glc}\% \approx 400\%$ and $\Delta CMR_{O_2}\% \approx 270\%$ with concomitant increases in cerebral lactate (for a review see Siesjo, 1978). Similarly ^{1}H-MRS measurements of bicuculline-induced seizures in the anesthetized rabbit showed an increase in cerebral lactate by an order of magnitude during steady-state seizures (Prichard *et al*. 1987). Smaller transient changes have been observed by ^{1}H-MRS during physiological stimulation in awake humans (Prichard *et al*. 1991; Sappey-Marinier *et al*. 1992; Frahm *et al*. 1996).

In light of the uncoupling between $\Delta CMR_{Glc}\%$ and $\Delta CMR_{O_2}\%$ with activation, the question becomes how these observations can be reconciled with the findings that most of the ATP produced during non-stimulated anesthetized conditions comes from glucose oxidation (for a review see Rothman *et al*. 2002). Obviously a new additional mechanism is needed, one that reconciles the stimulus-induced increase in CMR_{Glc} over CMR_{O_2} with the idealized stoichiometries and mechanisms for oxidation of glucose.

8. Possible explanation for non-oxidative energetics contributions

The greater increase of CMR_{Glc} than of CMR_{O_2} during stimulation can be resolved by a recent proposal for the dynamic use of brain energy (Shulman *et al*. 2001a, b). The energy requirement following a single firing event – which includes the action potential, neurotransmitter release as well as recycling, and associated excitatory (and/or inhibitory) postsynaptic potentials takes place over several milliseconds – is high because of the immediate need for glutamate clearance (by astrocytic uptake) from the extracellular space (Fig. 2). This rapid need for energy following each firing event cannot be synchronous with slow oxidative breakdown of glucose. Under conditions of slow firing rates, phosphocreatine and ATP reserves are presumably able to provide an adequate temporal energy buffer following each firing event. However during rapid firing this reserve is not able to support the rapid energy requirements following bursts of spikes. In analogy with the energy sources for muscular contraction (Shulman & Rothman, 2001), it has been proposed that the intense short term requirements for power required by these bursts of neuronal activity must be produced by rapid non-oxidative glycolysis or glycogenolysis (Shulman *et al*. 2001a, b).

https://doi.org/10.1017/S0033583502003803 Published online by Cambridge University Press

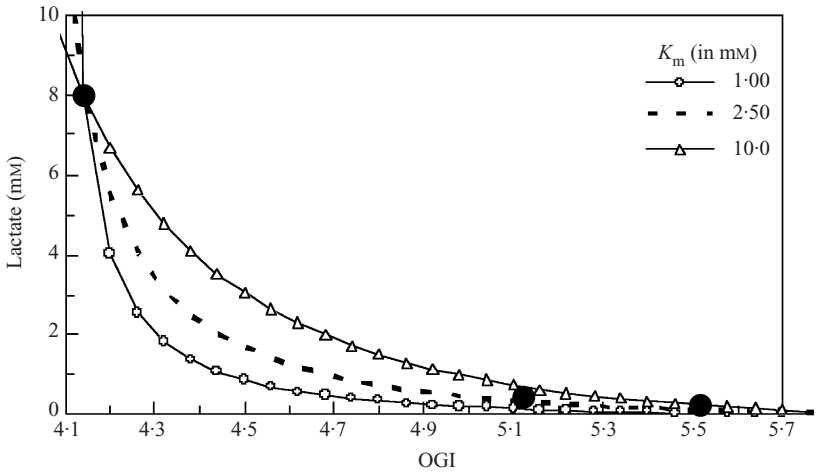


Fig. 5. OGI *versus* lactate dependence in the mammalian brain determined by Michaelis–Menten transport kinetics (see Shulman *et al.* 2001b for details). The OGI data (●) are from the resting human/rat brain (OGI ≈ 5·52; Siesjo, 1978), physiological activation in human brain (OGI ≈ 5·16; Gjedde, 1997), and seizure activity in rat brain (OGI ≈ 4·14; Siesjo, 1978). The amount of lactate during bicuculine-induced seizure is ∼ 8 mM (rat brain; Siesjo, 1978), the non-stimulated awake condition lactate level is ∼ 0·6 mM (human brain; Shulman *et al.* 1993), and the stimulated lactate level is ∼ 1 mM (human brain; Prichard *et al.* 1991). The relationship of Eq. (4) can be derived from Michaelis–Menten transport (V_{max}, maximum transport rate; K_m, lactate concentration at half V_{max}). The best fit of the model to the scarce data is with K_m of 2·5 mM, which corresponds to V_{max} of about 0·75 μmol g^{-1} min^{-1}. (Modified from Shulman *et al.* 2001b.)

However, when averaged over relatively long times the energy is essentially all supplied by oxidation of glucose in both the slow- and fast-firing cases, with the non-oxidative contributions serving as a temporal buffer.

As a consequence of the need to meet the temporal requirements of energy during increased activity, more lactate is produced (presumably in the astrocyte) than is needed for oxidation (presumably in the neuron) (Fig. 2). To meet the power requirements at the millisecond timescale of neuronal firing, and to the extent that the oxidative process shown in Fig. 2 is the energy supply, the excess lactate would be transported across the blood–brain barrier by mono-carboxylic acid transporters. The passive transport of lactate is driven by its concentration so that a Michaelis–Menten kinetic relation can be established between lactate concentration and its efflux (Shulman *et al.* 2001a, b). The excess lactate transported (x in molar units) is linked to the oxygen-to-glucose index (OGI) which is given by the ratio of CMR_{O_2} and CMR_{Glc}

$$OGI = CMR_{O_2}/CMR_{Glc} = 6 - 3x. \quad (4)$$

Equation (4) shows that aerobic (i.e. $x = 0$) and anaerobic (i.e. $x = 1$) glucose breakdown would result in OGI values of 6 and 3, respectively, which are the maximum and minimum OGI values in the lactate afflux model. Extreme values of OGI (∼ 4·0) and lactate concentration (∼ 8·0 mM) during steady-state seizure in animal models have been observed (Siesjo, 1978). The limited data from visual stimulation and seizure are consistent with the proposed relationship between OGI and the observed concentrations of lactate (Fig. 5). Because excess lactate is transported across the blood–brain barrier, this proposal allows glucose oxidation to be maintained as the energetics of neuronal firing and glutamate cycling

https://doi.org/10.1017/S0033583502003803 Published online by Cambridge University Press

(Fig. 2) during stimulation although the metabolic inputs show an apparent uncoupling between CMR_{O_2} and CMR_{Glc}.

The unique feature of this proposal is that the increased CMR_{Glc} reflects power needs, i.e. the rate of energy consumption rather than steady-state energy needs. This role for non-oxidative metabolism allows steady-state energy measurements to provide insights into rapid millisecond events. Although brain stoichiometry, as measured by inputs, departs from that expected by glucose oxidation, it does not mean that the organism is functioning inefficiently because the lactate transported out of a region can, as proposed by the lactate shuttle (Shulman *et al*. 2001a, b), be oxidized elsewhere.

Since the brain has a very large appetite for oxygen where even transient deficiencies in oxygen delivery can cause significant and permanent tissue damage (Siesjo, 1978), it is highly unlikely that a localized region can only depend upon non-oxidative metabolism for long time periods. From a survey of metabolic studies of the awake human (Shulman *et al*. 2001a), most physiological stimuli decrease the OGI value by $\sim 5\%$, whereas seizures decrease the OGI value by an additional 25%. Hence even in the extreme case of seizures the averaged energy needs are still supplied mainly by oxidative metabolism.

9. A model of total neuronal activity to support cerebral function

For technical reasons fMRI generally measures increments in regional brain activity. The ease of measuring incremental activity by functional imaging has been consonant with the widespread view that increments represent the modular energy required for functional activity (Posner & Raichle, 1998). However the high level of brain activity during non-stimulated conditions observed in the ^{13}C-MRS experiments has raised questions about considering cerebral function exclusively in terms of incremental activity (Shulman & Rothman, 1998). Furthermore a survey of ΔCMR_{Glc}% values (and spiking activity) revealed that for a particular stimulus, the deeper the anesthesia the larger the increment, leading to the suggestion that the total energy rather than the increment was needed for function (Shulman *et al*. 1999).

Recent experiments (Smith *et al*. 2002; Hyder *et al*. 2002) measured localized increments in CMR_{O_2} and in ν during sensory stimulation in α-chloralose-anesthetized rats. They addressed the following question: Does a cortical region require total or incremental neuronal activity to process sensory information? If increments in CMR_{O_2} and ν provide sufficient support for the neuronal activity processing sensory stimulation, then these increments should be independent of the basal activity level. Alternatively, if the neuronal activity requires particular magnitudes of CMR_{O_2} and ν then their increments should be larger from deeper anesthesia (Fig. 6).

Portions of the study which measured localized increments in CMR_{O_2} and ν during sensory stimulation in α-chloralose anesthetized rats are summarized in Appendix D. The basal levels were obtained by different depths of α-chloralose anesthesia, and in both conditions the same forepaw stimulation was used. In both conditions, stimulation produced approximately the same total magnitude of activity in both CMR_{O_2} and ν, while the increments varied accordingly, being larger from the lower basal level (Fig. 7). The data of CMR_{O_2} and ν plotted in Fig. 7 (see Appendix D for details) were normalized to their values at basal activity during light anesthesia. For both CMR_{O_2} and ν the basal activities were lower at deep anesthesia than at light anesthesia but the levels reached upon stimulation

https://doi.org/10.1017/S0033583502003803 Published online by Cambridge University Press

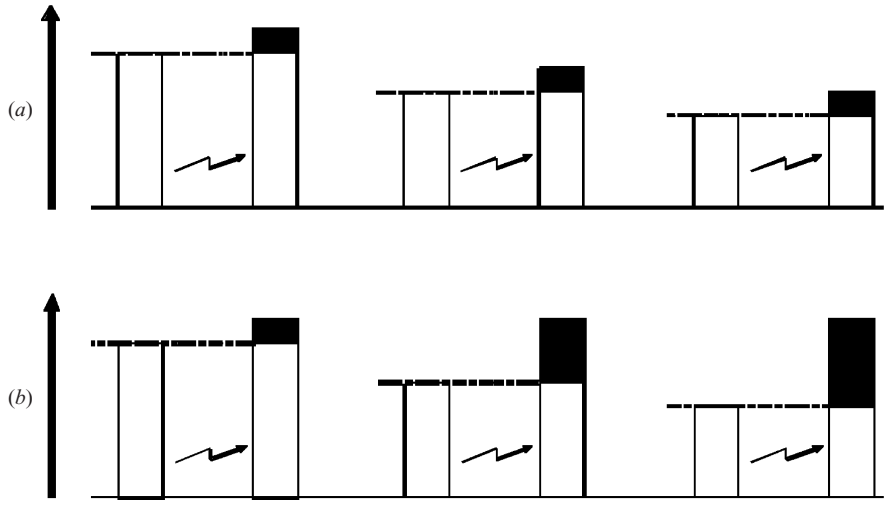


Fig. 6. Two possible models of non-stimulated baseline (white) and stimulation-induced incremental (black) activities are shown in (*a*) and (*b*), respectively. The jagged and vertical arrows represent the stimulation (same stimulus in all cases) and experimental parameters of neuronal activity are plotted vertically (same scale in all cases). (*a*) Stimulation induces the same increment in all cases, irrespective of the basal activity level. In this case only the *incremental* activity contributes to information encoding. (*b*) Stimulation induces an increment which depends on the baseline, being larger from a lower basal activity level. Here the *total* activity (i.e. baseline activity + incremental activity) is required for information encoding.

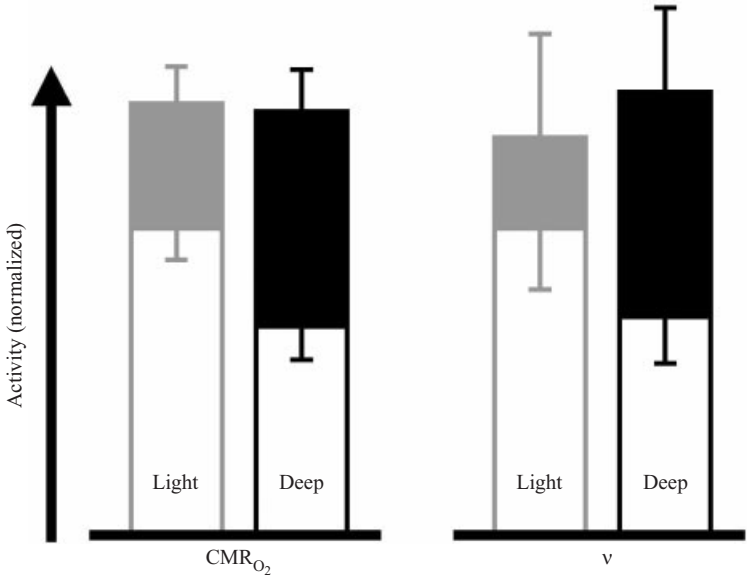


Fig. 7. The changes in CMR_{O_2} and ν relative to the non-stimulated baseline condition of light anesthesia (α-chloralose). While the increments (filled) of CMR_{O_2} and ν were different in light (gray) and deep (black) anesthesia levels, the same total activity levels were reached upon stimulation, where the size of the increment was dependent on the baseline level (open). See Fig. 6*b* for support and significance. The incremental changes (filled) can be directly compared to the data shown in Fig. 4. (Adapted from Hyder *et al.* 2002.)

https://doi.org/10.1017/S0033583502003803 Published online by Cambridge University Press

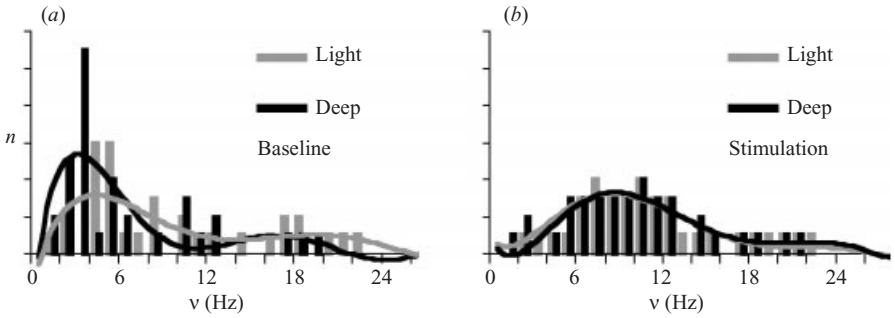


Fig. 8. The neuronal activity patterns, as reflected by spiking frequency (ν), of a small ensemble (72 neurons) from the somatosensory cortex in α-chloralose-anesthetized rats for four different conditions: (*a*) two baseline conditions and (*b*) two stimulated conditions. Each bar in the histogram represents averaged value of ν for that rat for the baseline (gray) and stimulated (black) conditions. The experimental protocol is summarized in Appendix D as well as Figs. 4 and 7. There is a significant difference between spiking frequency distributions in the two baseline conditions ($P < 0{\cdot}01$), whereas upon stimulation the spiking frequency distributions become similar ($P > 0{\cdot}25$). (Adapted from Smith *et al*. 2002.)

were approximately equal, and equality was reached (in both cases) by larger increases during stimulation from the lower basal level. The results in Fig. 7 are consistent with the ^{13}C-MRS results of high brain activity during non-stimulated basal conditions (Fig. 3).

Using energy as the measure of neuronal activity, the size of stimulus-induced incremental activity in awake human experiments is smaller than the basal activity. In anesthetized animals the size of incremental and basal activities depend on depth of anesthesia and can be as large as 200 % (for a review see Shulman *et al*. 1999). Therefore, the focus on only the magnitude of incremental activity neglects contributions of the basal activity (Shulman & Rothman, 1998) and can be misleading (Posner & Raichle, 1998). For example, if $\Delta CMR_{O_2}/CMR_{O_2}$ in a localized region for one cognitive task is 1 % (a typical value at 3 T) and for another task it is 2 %, it would be misleading to conclude that twice the neuronal activity is required in the second task. Assuming that approximately 75 % of CMR_{O_2} is associated with neuronal activity in humans (Shen *et al*. 1999; Lebon *et al*. 2002), a more accurate conclusion would be an increase in neuronal activity from 76 to 77 %.

Present results are in good agreement with an earlier report (Shulman *et al*. 1999) which showed that a particular total amount of activity is required for a stimulus to be processed under anesthesia, which in turn explained the large increments reported in neuroimaging studies of anesthetized animal (Ueki *et al*. 1988; Hyder *et al*. 1997). To respond to the stimulus, the energy is raised from the non-stimulated anesthetized levels to a total energy above or near the non-stimulated awake levels (Santori *et al*. 1986; Ueki *et al*. 1992; Hyder *et al*. 1996). The high levels of activity required for function have been supported by the present results, under the more reliable conditions of same animal, same stimulation, and same anesthetic at different doses.

The nature of neuronal response from the ensemble is depicted in Fig. 8. The comparison of spiking frequency histograms in the baseline conditions in Fig. 8*a* shows that in deeper anesthesia the frequencies are lower than at light anesthesia, with a population at the lower frequencies making a significant contribution to the difference. In accordance with the similar total energies during stimulation, comparison of spiking frequency histograms during stimulation (Fig. 8*b*) shows that not only are the average frequencies of the two states the

https://doi.org/10.1017/S0033583502003803 Published online by Cambridge University Press

same but that the distributions are also very similar. This similar distribution has been reached by a redeployment of many neurons in the ensemble. As shown in Appendix D a large majority of neurons change their firing rate upon stimulation – most increase their rate while non-negligible minorities either decrease or remain constant. The changes in total activity are effected by widespread changes in neuronal firing patterns of the ensemble.

Consequences of the large baseline activity (quantitated from ^{13}C-MRS studies) for interpreting neuroimaging data have been discussed previously (Shulman & Rothman, 1998). This interpretation explained the negative neuroimaging signals, sometimes observed with fMRI, which at that time had been considered an anomaly. Raichle (1998) had previously noted that negative signals were not expected on the prevailing view of brain function as inferred from the differencing approach used in functional imaging. On the basis of high brain activity during non-stimulated conditions, negative signals in a localized region were readily interpreted as a reduction in regional activity (in the stimulation period) (Shulman & Rothman, 1998). More recently, the existence and the importance of significant neuronal activity during non-stimulated conditions as a special property of certain brain regions (based on a meta-analysis of neuroimaging data) has been recognized by Gusnard & Raichle (2001). Implications for the interpretation of neuroimaging data, many of which have been suggested previously (Shulman & Rothman, 1998; Shulman *et al*. 1999) can now be extended.

10. Implications for interpretation of fMRI studies

To date, the predominant application of fMRI is for creation of 'horizontal' maps which locate regions of increased activity induced by specific sensory or psychological stimuli. This approach requires the subtraction of an important and required baseline activity, which as discussed above (Figs. 6 and 7) removes an important part of the total activity that is required for cerebral function. A neglected application of fMRI is the need to understand and quantify the 'vertical' maps which provide information about the degree of neuronal activity induced by the stimuli. The present biophysical perspective of fMRI studies, which derives the fundamental parameter of neural work (i.e. CMR_{O_2}) from BOLD data, can help to bridge this information gap.

This undertaking is accomplished by calibrating the fMRI method, which in practice combines separate MRI measurements of CBF, CBV, and BOLD signal (for a review see Hyder *et al*. 2001). Absolute and relative values of CBF (for a review see Calamante *et al*. 1999) can be obtained along with BOLD measurements merely by slightly modifying MRI pulse sequences, while measurement of relative CBV can be obtained by the same methods in conjunction with an exogenous paramagnetic contrast agent (for a review see Kennan *et al*. 1997).

A summary of the BOLD calibration for determining ΔCMR_{O_2}% in the rat brain is shown in Appendix C. Of all the parameters that influence the BOLD signal, the changes in CBV have the smallest impact. If the negligible effects of ΔCBV% on ΔS% are ignored, then fMRI image contrast [see Eq. (C 4)] can be determined from the pseudo-linear relationship between CBF and CMR_{O_2} (Hyde *et al*. 1998, 2000). Since the calculated values of ΔCMR_{O_2}% (from BOLD) have been confirmed by comparison with measured values of ΔCMR_{O_2}% (from ^{13}C-MRS), the combined used of CBF, CBV, and BOLD methods can be used to quantify localized changes in CMR_{O_2}. Recent results show that ΔS% is linked to neurotransmitter release (Kida *et al*. 2001) and neuronal firing (Smith 2002 In Press) at the

https://doi.org/10.1017/S0033583502003803 Published online by Cambridge University Press

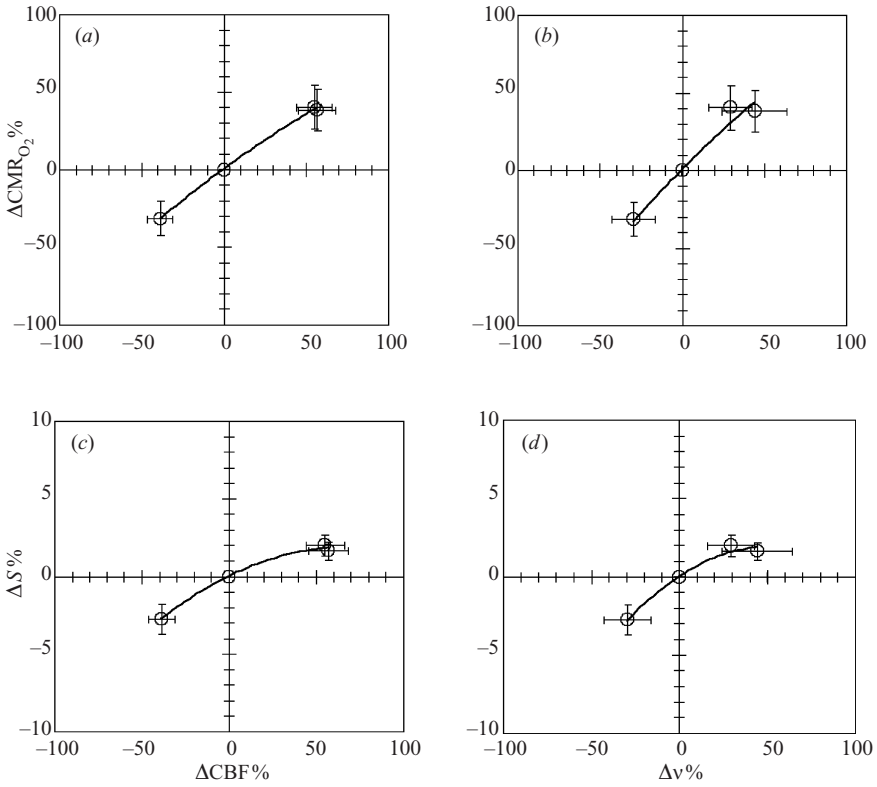


Fig. 9. Neurophysiological basis of fMRI. Relationships between stimulation-induced changes in (*a*) CMR_{O_2} and CBF, (*b*) CMR_{O_2} and ν, (*c*) S and CBF, and (*d*) S and ν. The data were obtained from α-chloralose-anesthetized rats during forepaw stimulation (Hyder *et al.* 2002; Smith *et al.* 2002). Over the entire range of activities measured, the relationship for CMR_{O_2} with CBF (*a*) and ν (*b*) are near-linear, whereas the relationships for S with CBF (*c*) and ν (*d*) are nonlinear. ΔCMR_{O_2}% is approximately proportional to ΔCBF% and $\Delta\nu$% and all three are of the same order of magnitude. ΔS% is smaller by an order of magnitude than ΔCBF% and $\Delta\nu$%. To interpret the BOLD signal in terms of function, ΔCMR_{O_2}% can be seen to depict the magnitude of $\Delta\nu$% accurately.

glutamatergic synapse in rat cerebral cortex, thereby establishing a strong foundation for the neurophysiological basis of BOLD (Hyder *et al.* 2002).

The neurophysiological insight of fMRI image contrast is gained by cross comparison of the multi-modal data of ΔCMR_{O_2}%, ΔCBF%, $\Delta\nu$%, and ΔS% (Fig. 9). The data in Fig. 9 were obtained from α-chloralose-anesthetized rats during forepaw stimulation (Hyder *et al.* 2002; Smith *et al.* 2002). Over the entire range of activities measured, ΔCMR_{O_2}% is proportional to both ΔCBF% and $\Delta\nu$% whereas in contrast ΔS% is smaller by an order of magnitude and is not proportional to $\Delta\nu$%. Since the magnitudes of ΔS% and $\Delta\nu$% are not proportional to each other, quantitative use of fMRI for imaging neuronal activity depends upon deriving ΔCMR_{O_2}% from BOLD to depict the magnitude of $\Delta\nu$%.

11. The restless brain

The functional integrity of the brain depends on a collection of active cells which are continuously transferring and processing information. Glucose oxidation provides most of

https://doi.org/10.1017/S0033583502003803 Published online by Cambridge University Press

the energy for this work (Siejso, 1978). The term 'work' is defined here as the sum of the energy-consuming processes associated with neuronal activity. The energetic demands of the cells are extremely high – as noted earlier that in the awake human brain $\sim 20\%$ of the total body's energy from oxygen consumption is consumed in the brain, which by weight is only $\sim 2\%$ of the total body mass (Sokoloff, 1991). Our NMR studies have investigated the relationship between neuroenergetics and neurotransmission in animal models. Our major findings can be summarized as follows:

- Changes in energy consumed and flux of glutamate neurotransmission are highly correlated over a wide range of cerebral activity (Figs. 3 and 4).
- The glutamate neurotransmitter flux can be determined from the correlation with the energy, usually measured as $\Delta CMR_{O_2}\%$ [Eq. (3)].
- In the awake non-stimulated condition (i.e. baseline activity), more than two thirds of the energy is devoted to neuronal activity [Eq. (1)].
- The neuronal activity and energy consumption associated with sensory stimulation reach the same values regardless of the baseline values (Figs. 7 and 8).
- The total neuronal activity and associated energy consumption in a region is required for brain function (Figs. 7 and 8).

For a variety of technical reasons, the conventional use of PET and fMRI methods rely on incremental signals to localize regions activated by the stimulus. In cases where the baseline is well defined (e.g. sensory stimulation), difference mapping has localized responses to stimulation with great validity and reliability based upon correlations with many electrophysiological measures (e.g. action and field potentials). Whereas difference maps of sensory modalities in non-human primates reinforce and extend understanding of the sensory pathways (Disbrow *et al*. 2001; Bush *et al*. 2002; Tolias *et al*. 2002), cognitive modalities are more difficult to correlate mainly due to the ambiguous definition of baseline in most tasks. In the less well understood areas of cognition, the use of a differencing approach, while not at the conclusive level found in sensory modalities, still provides reliable localization of *some* function. There is no doubt that differencing signals meaningfully localize changes in activities, and our findings do not contradict such localizations, however we do question the meaningfulness of *only* using increments and discarding the important baseline signal. Our findings challenge cognitive neuroscience studies, where it is generally assumed that incremental activity alone is responsible for information processing (for a review see Posner & Raichle, 1998).

We propose that the goal of neuroimaging methods should be to quantitatively measure both the baseline and incremental signals. NMR methods can provide quantitative estimates of both signals which represent activities of a very large population of neurons. In contrast, the signals measured by electrophysiological methods are at the level of individual or a few cells. Recent electrophysiological studies suggest that the collaboration amongst a large number of neurons, some of which are firing faster and others slower, is crucial for encoding information in the brain (for a review see Scannell & Young, 1999). The idea that a certain number of neurons in a cortical region respond to a given stimulus (i.e. population voting) is not new. It was suggested long ago by E. D. Adrian who observed that touch causes discharges in several nerve fibers, with relative intensities that in turn map the stimulus onto the cortex (for a review see Kandel *et al*. 1991). Therefore, information of the world is more

https://doi.org/10.1017/S0033583502003803 Published online by Cambridge University Press

likely to be encoded in the brain by neuronal populations rather than by actions of individual neurons (for a review see Kristan & Shaw, 1997) because typically each cell responds to more than one stimulus variable (e.g. intensity, frequency, etc.), and an individual cell cannot distinguish amongst these different stimulus variables. Since the response profiles of neurons are different, and a single neuron does not participate in just one type of function, the firing of a single cell by itself does not provide a meaningful basic code for information processing (for a review see Chapin & Nicolelis, 1999).

Our recent fMRI studies combined with electrophysiology (Hyder *et al*. 2002; Smith *et al*. 2002), which measured the firing rates of a neuronal population and their energy consumption, provide insight into the population voting of 72 neurons (Fig. 8; Appendix D). Within the precision of the present measurements in which energy consumption and firing rates increase proportionately [Fig. 4; Eq. (2)], there are significant contributions to the energy from quiescent neurons (Fig. 16; Appendix D). Since about one third of the population (from deeper anesthesia level) did not respond to the stimulus, the incremental energies (from calibrated BOLD) during stimulation represent the distributed voting choices of the population of neurons. The histograms of firing rates (Fig. 8) depict the redeployment of the same neurons as a function of stimulated and non-stimulated conditions. While this redistribution of the population voting is usually measured as an increment by neuroimaging techniques, the total energies in the two conditions represent the integrated activities of the populations, and the increments represent their shifts.

The increment, therefore, is only conceptually separable from the total activity by comparing total activities of the population in two states. Viewed as a general redeployment of neuronal firing frequencies, it is clear that the integrated signal from a region can be increased, decreased, or remain unchanged. The variations in firing patterns upon stimulation do not, at this time, comprise an understandable ensemble because we do not know exactly why the frequency of a specific neuron is increased while for another it is decreased. But we can surmise that these neurons may be respectively classified as excitatory pyramidal cells and inhibitory inter-neurons based on neuroanatomy (Shepherd, 1994). While the distributions of firing rates during non-stimulated conditions vary (Fig. 8*a*), the distributions of firing rates during a particular stimulation in our limited experiments seem to be characteristic of that state, thus allowing the possibility that a particular population is a consequence of the same total energy being required during a particular stimulation, regardless of the starting baseline activity (Fig. 8*b*). More detailed studies of neuronal populations in non-human primate models (Desimone, 1996; Goldman-Rakic, 1996; Tanaka, 1996; Georgopoulos, 2000; Logothetis, 2000; Rolls, 2000) will be needed for extensions to cognitive function in the awake human brain.

The total energy consumption, above levels at isoelectricity, in a voxel has been related to the rates of total neuronal firing (Fig. 4) and neurotransmitter release (Fig. 3) by the experiments reviewed above. These neuronal functions and their energy consumption are located in the neuropil (Sokoloff, 1993, 1999), distributed between pre- and postsynaptic terminals (Attwell & Laughlin, 2001). Hence the total energy derived from the fMRI signal is coupled to the total synaptic activity in the voxel. In the present extracellular recordings, the electrodes selected activities of neurons in layer 4, many of which form thalamo-cortical connections (Shepherd, 1994). Additional experiments could explore the energy consumption of specific cortical layers.

Two recent experiments interpreted in terms of high baseline activity are consistent with

https://doi.org/10.1017/S0033583502003803 Published online by Cambridge University Press

the important role assigned the total activity in our discussion. The need for substantial unfocussed neuronal activity for the service of sensory responses was suggested from experiments by Grinvald and colleagues (Tsodyks *et al*. 1999) who studied the correlation between single neuron activity measured by electrophysiology and total ensemble activity measured by optical methods. From single-unit recordings they recognized that 'cortical neurons are spontaneously active in the absence of external input even in primary sensory areas'. From real-time optical imaging experiments they concluded that 'in the absence of stimulation the cortical network wanders through various states represented by coherent firing of different neuronal assemblies' and that a stimulus pushes the network into a limited number of these states representing the stimulus. Grinvald and colleagues recognized the high level of non-stimulated neuronal activity and suggested that the ensemble activity is reorganized during stimulation, where the redeployment of the large baseline activity was proposed to support the stimulation – as we have documented at the neuronal level (Figs. 7 and 8). Analogously the temporal synchronization of neuronal responses in the visual system measured by Singer and colleagues have led these authors to conclude that 'of the many responses of V1, those that become synchronized best will be particularly effective in influencing neurons in higher areas' (Singer, 1994). Both studies support the presence of high neuronal activity in the non-stimulated state, and suggest a role for the large baseline activity in brain function. Our studies provide quantitative measures of the total amount of the stimulated and non-stimulated activities in a region, and thereby provide a unique quantitative basis for evaluating theories regarding the significance of baseline activity.

Our ^{13}C-MRS measurements of the brain show high activity in the absence of strong external stimuli for the awake condition (Fig. 3). The resting baseline activity is the sum of energy-consuming connections measured in the voxel between neurons of different types. In addition to local inter-neurons the synaptic activity in a voxel responds to connections with the rest of the brain (Braitenberg & Schuz, 1991). These remote neuronal connections, which support the de-localized aspects of brain activity, should contribute to our measures of total activity. The total neuronal activity, which arises from both local and distal neurons, are reduced by anesthesia (Ueki *et al*. 1988; Hyder *et al*. 1996) *both* inside and outside of the somatosensory region. Upon stimulation, the total neuronal activity inside the region of interest becomes high, and comparable to the activity at rest in the non-anesthetized awake condition, whereas total neuronal activity outside the stimulated region remains low (Ueki *et al*. 1992; Hyder *et al*. 1997). Thus the forepaw stimulation introduces additional neuronal activity to the low baseline activity in the somatosensory cortex. However, in a non-anesthetized functional experiment the situation may be slightly different. In the non-anesthetized awake brain at rest (Sokoloff *et al*. 1977), the forepaw stimulation introduces a small additional neuronal activity thereby raising the total neuronal activity only slightly above the non-anesthetized awake resting state (Shulman *et al*. 1999; Hyder *et al*. 2002). In this case, the fractional increase would be smaller. This interplay between contributions from localized and de-localized neuronal connections provides insight to important questions of brain organization.

One relevant neuroscientific framework for relating localized and widespread activities has been offered and developed by Changeux and colleagues (Dehaene *et al*. 1998). The participation of large neuronal populations in function was assumed from measurements of electrical activity in awake and asleep humans (Changeux, 1985). The authors conceptually divide neuronal activity into a specific localized response to brain tasks (e.g. forepaw

https://doi.org/10.1017/S0033583502003803 Published online by Cambridge University Press

stimulation) interacting with a more de-localized response that modulates and controls the specific response. They define the de-localized activity as a *global workspace* that can 'potentially interconnect multiple distributed and specialized brain areas in a coordinated, though variable manner, and whose intense mobilization might be associated with a subjective feeling of conscious effort'. The authors propose the *global workspace* to be active when, in addition to the specific modules, a stimulus mobilizes other brain regions.

Since the baseline activity measured from layer 4 in our studies (Fig. 8) is comprised of signals from local inter-neurons as well as from distal neurons (Shepherd, 1994), the large baseline activity (Fig. 3) could therefore be identified as input from and connections to other neurons including those in regions of the *global workspace*. The widespread decrease of baseline activity in the anesthetized state must produce a decrease in global activity. Since anesthesia induces slow axonal conduction of most neurons (Richard, 1998), the reduction of *global workspace* is consistent with the state of depressed activity during non-stimulated anesthetized states. Because the rest of the brain does not respond to forepaw stimulation and remains at low anesthetized activity, we conclude that connections with the *global workspace* are reduced during stimulation in the anesthetized state. Therefore the localized total neuronal activity in the somatosensory cortex must include sizeable contributions from the sensory neurons. We cannot, of course, define the overall response of the ensemble to the stimulus, but as judged by the lack of the rat's motor response and the depressed brain activity there is no reason to consider that the animal is 'cognitively' responding in ways that can be monitored by the *global workspace*. Since contributions of individual neurons in the voting population can be evaluated, the activity patterns during stimulated and non-stimulated conditions from anesthesia can be distinguished in future studies. The *global workspace* is assigned in this proposal to the neuronal energies interfacing with the widespread neuronal activities that support subjective experiences, i.e. the baseline activities, required for subjectivity. These assignments of total energetics and activities, measured by fMRI experiments as described in this paper, provide quantitative measures that will help separate local from global responses.

12. Acknowledgements

We gratefully acknowledge grant support from the National Institutes of Health grants NS-32126 (D. L. R.), NS-37203 (F. H.), DC-003710 (F. H.), DK-27121 (R. G. S.), MH-67528 (F. H.); National Science Foundation grants DBI-9730892 (F. H.), DBI-0095173 (F. H.).

13. Appendix A. CMR_{O_2} by ^{13}C-MRS

^{13}C-MRS provides a unique window on cerebral metabolism *in vivo* (Shulman *et al*. 1993). The Larmour frequency of the ^{13}C nucleus responds to electronic environments within a molecule, allowing non-invasive assignment of ^{13}C resonances with high spectral resolution from specific positions within molecules, e.g. glucose, glutamate, glutamine, GABA, aspartate. Since the natural abundance of the ^{13}C isotope is only 1·1 %, the sensitivity of ^{13}C-MRS can be enhanced using ^{13}C-enriched substrates (Rothman *et al*. 1999). Intravenous infusion of enriched ^{13}C-labeled glucose allows the subsequent appearance of the ^{13}C label in specific products of cerebral glucose metabolism to be measured in real time (Fig. 10).

https://doi.org/10.1017/S0033583502003803 Published online by Cambridge University Press

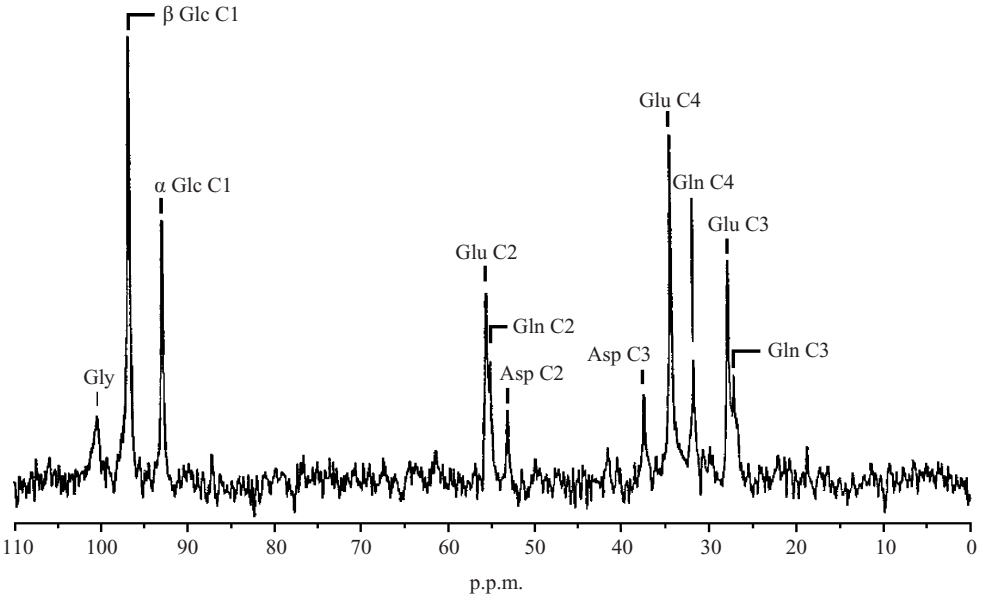


Fig. 10. Intravenous infusion of ^{13}C-labeled glucose results in time-dependent appearance of ^{13}C label into specific products of glucose metabolism. In the mammalian brain, two major 'sinks' for ^{13}C are the glutamate and glutamine pools. The *in vivo* spectrum was obtained at 7 T from a localized gray matter volume (300 μl; 10-min average) of an α-chloralose-anesthetized rat brain after 2 h infusion of [1-^{13}C]glucose. Abbreviations: Asp, aspartate; Glc, glucose (α and β anomers); Gly, glycogen; Glu, glutamate; Gln, glutamine. (Adapted from Hyder *et al*. 2001.)

Observations of ^{13}C label flow from glucose to metabolite pools have been used to estimate a range of metabolic fluxes *in vivo* in absolute units of μmol g^{-1} min^{-1} (Fitzpatrick *et al*. 1990; Mason *et al*. 1992; Hyder *et al*. 1996; Sibson *et al*. 1997). ^{13}C label flow measurements have been used to measure important neurophysiological fluxes, e.g. TCA cycle (V_{TCA}), glutamate–glutamine cycling (V_{cyc}), glucose oxidation ($CMR_{Glc(ox)}$), and oxygen consumption (CMR_{O_2}).

The time-course of ^{13}C isotopic labeling of [4-^{13}C]glutamate arising from the infusion of [1-^{13}C]glucose has been used in combination with mathematical models of isotopic exchange in metabolite pools to calculate V_{TCA} (Mason *et al*. 1992, 1995). Upon infusing [1-^{13}C]glucose the glutamate pool is labeled at C4 in the first turn of the TCA cycle, and at C3 or C2 subsequently. The initial formulation of the model (Mason *et al*. 1992) considered 9 metabolite pools, 13 isotopically labeled substances, and 9 metabolic fluxes. A simpler model (Fig. 11) has been used recently (Mason *et al*. 1995) to measure V_{TCA} (Fig. 11, inset) in rat brain during forepaw stimulation (Hyder *et al*. 1996, 1997, 2000). This metabolic model is expressed as a system of coupled, first-order, linear ordinary differential equations as follows (see legend to Fig. 11 for definitions):

$$d[\mathrm{L}^*]/\mathrm{d}t = -(V_{TCA} + V_{dil})[\mathrm{L}^*]/[\mathrm{L}] + 2\mathrm{CMR}_{Glc}[G^*(t)]/[G(t)], \quad \text{(A 1)}$$

$$d[\mathrm{Glu\ C4}^*]/\mathrm{d}t = V_{TCA}[\mathrm{L}^*]/[\mathrm{L}] - (V_{TCA} + V_{Gln})[\mathrm{Glu\ C4}^*]/[\mathrm{Glu\ C4}] + \mathrm{V}_{Gln}[\mathrm{Gln\ C4}^*]/[\mathrm{Gln\ C4}], \quad \text{(A 2)}$$

$$d[\mathrm{Gln\ C4}^*]/\mathrm{d}t = V_{Gln}[\mathrm{Glu\ C4}^*]/[\mathrm{Glu\ C4}] - V_{Gln}[\mathrm{Gln\ C4}^*]/[\mathrm{Gln\ C4}], \quad \text{(A 3)}$$

https://doi.org/10.1017/S0033583502003803 Published online by Cambridge University Press

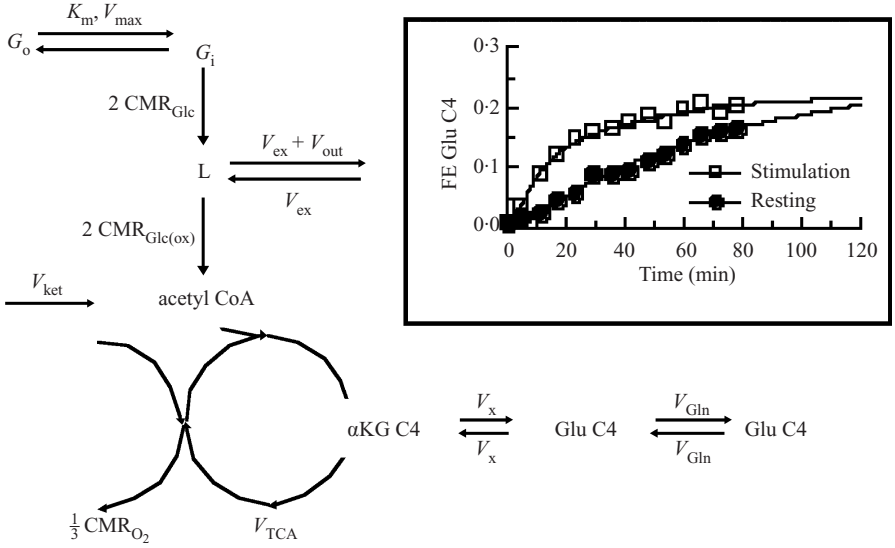


Fig. 11. Metabolic model schematic of isotopic mass balance at steady state (see Mason *et al*. 1992, 1995 for details). The [1-^{13}C]glucose in plasma (G_o) and brain (G_i) exchange via Michaelis–Menten kinetics (K_m = half-saturation concentration for transport; V_{max} = maximum transport rate). The ^{13}C label flows at the rate 2 CMR_{Glc} through glycolytic intermediates (negligible concentrations) and arrives at pyruvate C3 and lactate C3, which is represented by L (1·5 μmol g^{-1}). Two sources of ^{12}C entry into the TCA cycle are exchange of blood–brain pyruvate and lactate pool (V_{ex}) and the ketone body flux (V_{ket}), both of which dilute the ^{13}C fractional enrichment ($V_{dil} = V_{ex}$ or V_{ket}) of intermediates. The efflux at L (V_{out}) causes some ^{13}C label to be lost to blood. The ^{13}C label enters the acetyl CoA pool at a rate of 2 $CMR_{Glc(ox)}$ prior to its entry into the TCA cycle. The ^{13}C label enters the TCA cycle and labels α-ketoglutarate C4 (αKG C4), and glutamate C4 (Glu C4) (12·0 μmol g^{-1}). These two pools are in very rapid isotopic exchange, V_x, where $V_x/V_{TCA} \gg 1$. There is an exchange between glutamate C4 and glutamine C4 (Gln C4) (6·2 μmol g^{-1}), at a rate of V_{Gln} (where V_{Gln}/V_{TCA} ranges from 1/4 to 1). CMR_{O_2} is equal to 3 V_{TCA} −3/4 V_{dil}. *Inset:* ^{13}C turnover fractional enrichment (FE) of glutamate C4 data from anesthetized rat brain (symbols) and best fits of the metabolic model (lines) for steady-state conditions of resting (circle) and stimulation (box) obtained by ^{1}H-[^{13}C]MRS at 7 T (24 μl; PoCE; 5-min average). The comparison demonstrates that V_{TCA} is significantly increased during forepaw stimulation (0·3 ms pulses; 2 mA amplitude; 3 Hz) of the rat with α-chloralose anesthesia. (Adapted from Hyder *et al*. 1997.)

where metabolite concentrations (shown within [ ]) with and without the symbol * represent the enriched (^{13}C only) and total (^{13}C+^{12}C) pools, respectively. The value of V_{TCA} is estimated with the model by minimizing the least-squares differences between the measured time course of [Glu C4*]/[Glu C4] and the corresponding values of [Glu C4*]/[Glu C4] calculated from Eqs. (A 1)–(A 3) given the measured time-course of $[G^*(t)]/[G(t)]$ as a function of V_{TCA}. The precision of V_{TCA} is estimated by adding random noise to the best fit for the time-course of [Glu C4*]/[Glu C4] and reassessing V_{TCA} in a Monte Carlo fashion.

Since there is a textbook stoichiometry between the TCA cycle flux and oxidative phosphorylation, $CMR_{Glc(ox)}$ and CMR_{O_2} can be calculated from these experiments. In the particularly simple case of [1,6-^{13}C]glucose, where both pyruvates will be labeled, the relationship is

$$CMR_{Glc(ox)} = \tfrac{1}{2}[\tfrac{3}{4} + \tfrac{1}{4}(Glu^\bullet/Glc^\bullet)]V_{TCA}, \quad \text{(A 4)}$$

$$CMR_{O_2} = [2\tfrac{1}{4} + \tfrac{3}{4}(Glu^\bullet/Glc^\bullet)]V_{TCA}, \quad \text{(A 5)}$$

https://doi.org/10.1017/S0033583502003803 Published online by Cambridge University Press

where $Glu^{\bullet}$ and $Glc^{\bullet}$ are the ^{13}C fractional enrichments of glutamate C4 and glucose C1,C6 respectively. Eqs. (A 4) and (A 5) show that if the ^{13}C fractional enrichments of glutamate C4 and glucose C1,C6 (in a [1,6-^{13}C]glucose infusion study) are equal, then $CMR_{Glc(ox)}$ and CMR_{O_2} are simply one-half and three times V_{TCA}, respectively. Since in reality $Glu^{\bullet} < Glc^{\bullet}$ over a wide range of activity (Hyder *et al*. 1996; Sibson *et al*. 1997), a small but measurable dilution term [see V_{dil} in Fig. 11 which is equal to $(1-Glu^{\bullet}/Glc^{\bullet})V_{TCA}$] is included in calculating $CMR_{Glc(ox)}$ and CMR_{O_2} (see Appendix B in Hyder *et al*. 2001). These experiments have also been used to estimate the rate of neurotransmitter cycling in glutamatergic neurons through labeling of glutamine C4 from glutamate C4 (see Appendix B).

14. Appendix B. V_{cyc} and test of model

From the assumption that neuronal glutamate is the sole precursor of glial glutamine, the time-courses of the ^{13}C-MRS signals can be used to calculate V_{cyc}, the rate of glutamate neurotransmitter cycling (Sibson *et al*. 1997), through labeling of glutamine C4 from glutamate C4 (Rothman *et al*. 1999). Since the glutamate C4 labeling time-course allows the determination of glucose oxidation ($CMR_{Glc(ox)}$), as shown in Appendix A. Simultaneous detection of C4 labeling in glutamate and glutamine (Fig. 3) reflect the stoichiometric relation between V_{cyc} and $CMR_{Glc(ox)}$ [see Eq. (1)]. Implications of Eq. (1) are central to our understanding and are discussed throughout the text. However before building upon this model, alternate explanations of the observed ^{13}C label flow must be satisfactorily eliminated or at least their contributions evaluated.

A stringent test of the glutamate-glutamine cycle model (Fig. 1) was performed by using different ^{13}C label sources. For example, [2-^{13}C]glucose should label C3 of glutamine before glutamate whereas [1-^{13}C]glucose should label C4 of glutamate before glutamine (see Fig. 12). However, both these different time-courses should give the same glutamate–glutamine cycle rate if the model (Fig. 1) is correct.

In the anesthetized rat, this prediction was tested by comparing the original [1-^{13}C]glucose labeling patterns with patterns obtained with [2-^{13}C]glucose (Sibson *et al*. 2001). The different labeling patterns expected from [1-^{13}C]glucose and [2-^{13}C]glucose are shown schematically in Fig 12. Briefly, [1-^{13}C]glucose infusion would label the C4 glutamate pool (i.e. mainly neuronal) first reflecting the pyruvate dehydrogenase activity, whereas [2-^{13}C]glucose infusion would label the C3 glutamine pool (i.e. mainly glial) first reflecting the pyruvate carboxylase activity. The *in vivo* results from such an experiment (Sibson *et al*. 2001) are shown in Fig. 13, where the observed ^{13}C-labeling patterns are in good agreement with theoretical expectations. Furthermore the glutamate cycling rates determined from both ^{13}C flow directions were equal within experimental errors. Similar experiments have been conducted in the awake human with [1-^{13}C]glucose (Shen *et al*. 1999) and [2-^{13}C]acetate (Lebon *et al*. 2002), which are believed to be preferential substrates of neurons and glia, respectively (Cerdan *et al*. 1990), and again the cycling rates determined from the two different label sources are in good agreement.

An alternate function for glutamine synthesis is ammonia detoxification, a process by which ammonia is cleared by glutamine efflux from the brain. This particular pathway was evaluated by measuring both the ^{13}C and ^{15}N label flows into glutamine at different levels of blood ammonia using ^{13}C-MRS and ^{15}N-MRS, respectively. The ^{13}C-MRS method has been described above. An indirect ^{15}N-MRS method for measuring ^{15}N-labeled compounds *in vivo*

https://doi.org/10.1017/S0033583502003803 Published online by Cambridge University Press

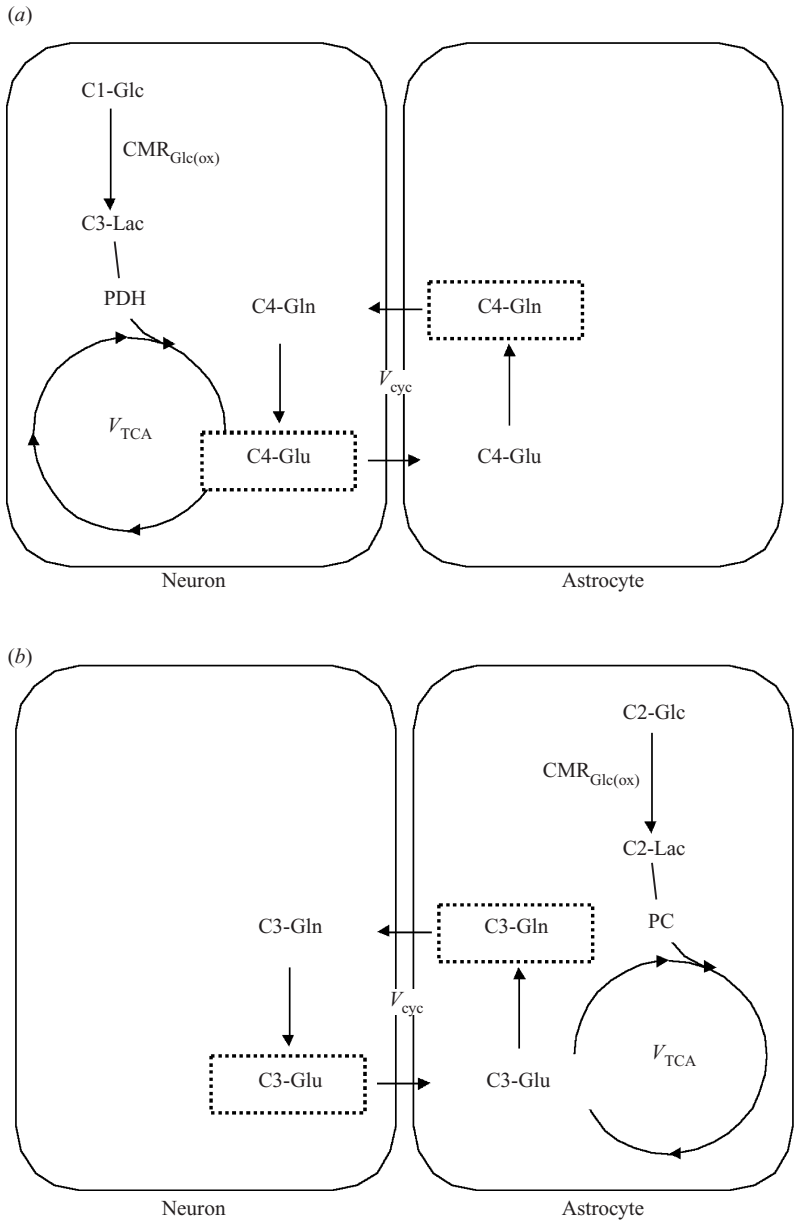


Fig. 12. (*a*) In the [1-^{13}C]glucose experiment, the ^{13}C label flows from glucose C1 to pyruvate C3 and lactate C3, and through the TCA cycle intermediates, into glutamate C4 due to fast isotopic exchange between glutamate C4 and α-ketoglutarate C4. Glutamate C4 in the neuron serves as a precursor for glutamine C4 in the astrocyte. Since glutamine C4 labeling lags behind glutamate C4 under these situations, the [1-^{13}C]glucose experiment mainly reflects neuronal pyruvate dehydrogenase (PDH) activity. (*b*) In the [2-^{13}C]glucose experiment, the ^{13}C label flows from glucose C2 to pyruvate C2 and lactate C2 and enters the TCA cycle resulting in glutamate C5 labeling. But this ^{13}C label is lost as $^{13}CO_2$ in the first turn of the TCA cycle via the pyruvate dehydrogenase reaction in the neuron. However, ^{13}C label can also lead to consequent C3 labeling in intermediates of the TCA cycle via the pyruvate carboxylase (PC) reaction in the astrocyte. Thus in the [2-^{13}C]glucose experiment glutamine C3 labeling is detected prior to C3 glutamate under steady-state conditions, which indicates that the [2-^{13}C]glucose experiment mainly reflects astrocytic pyruvate carboxylase activity. In both of these experiments the

https://doi.org/10.1017/S0033583502003803 Published online by Cambridge University Press

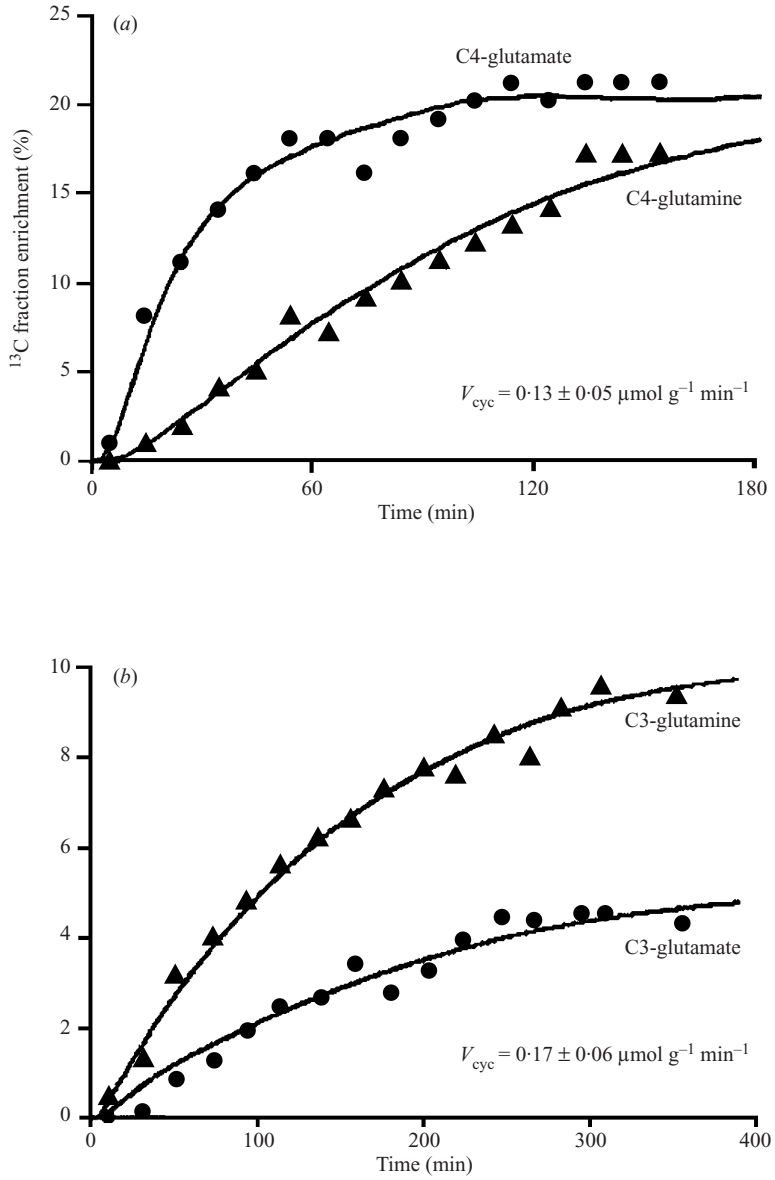


Fig. 13. (*a*) Typical ^{13}C labeling patterns for C4 of glutamate and glutamine observed during a [1-^{13}C] glucose infusion experiment. In this experiment, C4 of glutamate is the precursor of C4 of glutamine and under these conditions the [1-^{13}C]glucose experiment mainly reflects neuronal pyruvate dehydrogenase activity. (*b*) Typical ^{13}C-labeling patterns for C3 of glutamate and glutamine observed during a [2-^{13}C]glucose infusion experiment. In this experiment, C3 of glutamine is the precursor of C3 of glutamate and under these conditions the [2-^{13}C]glucose experiment mainly reflects neuronal pyruvate carboxylase activity. V_{cyc} in these two α-chloralose-anesthetized rats were estimated to be similar within experimental errors. (Adapted from Sibson *et al.* 2001.)

time lag observed between labeling of glutamate and glutamine can be modeled to determine the same glutamate–glutamine neurotransmitter flux (V_{cyc}), as shown in Fig. 13.

https://doi.org/10.1017/S0033583502003803 Published online by Cambridge University Press

was developed by Kanamori & Ross (1993, 1995) to follow the flow of ^{15}N from labeled ammonia into glutamate and glutamine. In the anesthetized rat brain, the measured value of glutamine synthesis ($0{\cdot}20 \pm 0{\cdot}06$ μmol g^{-1} min^{-1}) from ^{15}N MRS studies (Shen *et al*. 1998) agreed well with the value ($0{\cdot}21 \pm 0{\cdot}04$ μmol g^{-1} min^{-1}) obtained from ^{13}C-MRS studies (Sibson *et al*. 1997). Furthermore, both ^{13}C-MRS (Sibson *et al*. 1997) and ^{15}N-MRS (Shen *et al*. 1998) methods revealed that at normal ammonia levels, the rate of glutamine synthesis is approximately equal to the glutamate cycling flux, where the small corrections needed for ammonia detoxification could be neglected (Sibson *et al*. 1997; Shen *et al*. 1998; Rothman *et al*. 1999), thus simplifying the quantitation of V_{cyc} in human studies directly from ^{13}C-MRS measurements of C4 glutamate and glutamine labeling patterns (Shen *et al*. 1999; Lebon *et al*. 2002).

15. Appendix C. CMR_{O_2} by calibrated BOLD

The MRI signal (S) in spin-echo and gradient-echo image contrasts (i.e. the most commonly used MRI sequences) is dependent on transverse relaxation times of tissue water (i.e. $T_{2,\mathrm{tissue}}$ and $T^*_{2,\mathrm{tissue}}$, respectively)

$$S(TE) \propto \exp(-TE/T_2), \tag{C 1}$$

where TE is time of signal decay (the echo time) and T_2 can be either $T_{2,\mathrm{tissue}}$ or $T^*_{2,\mathrm{tissue}}$ from spin-echo or gradient-echo MRI sequences, respectively. Both spin-echo and gradient-echo images are affected by microscopic inhomogeneities of the static magnetic field (B_0).

Suppose that hemoglobin molecules are contained within a uniform cylinder of infinite length in a microvascular tissue unit. Since deoxyhemoglobin is paramagnetic, it creates local B_0 gradients within the capillary which extend into the surrounding tissue to affect the ^1H spins of tissue water molecules. These local B_0 gradients are a consequence of the difference in volume magnetic susceptibility between the capillary and tissue. For randomly oriented cylinders (that mimic the capillary network within tissues), the local B_0 gradients reduce $T_{2,\mathrm{tissue}}$ or $T^*_{2,\mathrm{tissue}}$ which decreases the MRI signal [see Eq. (C 1)]. This extravascular T_2 effect is present within each MRI voxel at macroscopic scale (Ogawa *et al*. 1993). The intravascular T_2 effect can be ignored at high B_0 because the T_2 of blood becomes very short and therefore the experiments mainly reflect the changes in T_2 of tissue (Ugurbil *et al*. 2000).

The BOLD image contrast indirectly reflects red blood cell hemoglobin oxygenation (Y) by the relaxation time of tissue water (Ogawa *et al*. 1993):

$$1/T_{2,\mathrm{tissue}} = C\nu_{\max}(1-Y)b\ \mathrm{Hct}, \tag{C 2}$$

where C is a proportionality constant, $\nu_{\max}$ is a B_0-dependent deoxyhemoglobin susceptibility frequency shift, b is the blood volume fraction, $(1-Y)$ is the blood deoxygenation, and Hct is the blood hematocrit. An increase in the fractional signal change ($\Delta S/S > 0$), as observed in a functional imaging experiment, is consistent with a drop in venous deoxyhemoglobin concentration, which leads to an increase in the transverse relaxation time of water in the tissues. The BOLD fMRI signal change observed with spin-echo image contrast at steady state is defined as

$$\Delta S/S = \exp(-\Delta(1/T_{2,\mathrm{tissue}}) \times TE) - 1, \tag{C 3}$$

For optimum contrast [i.e. highest value of Eq. (C 3)] the TE must equal $T_{2,\mathrm{tissue}}$. Similar equations can be written for the gradient echo, where $T_{2,\mathrm{tissue}}$ is replaced with $T^*_{2,\mathrm{tissue}}$ in Eqs.

https://doi.org/10.1017/S0033583502003803 Published online by Cambridge University Press

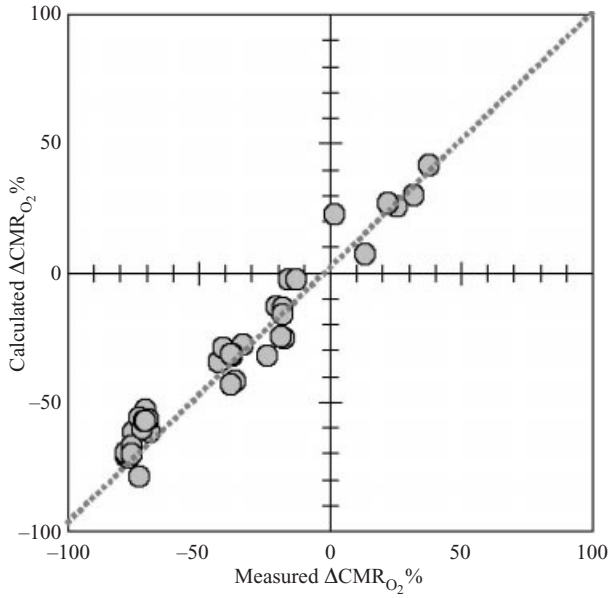


Fig. 14. In rat brain, quantitative MRI measurements of CBF, CBV, and BOLD signal, over a wide range of neuronal activity, have been used to calculate ΔCMR_{O_2}% from the calibrated BOLD at 7 T [where $\acute{A}$ in Eq. (C 4) is equal to $0{\cdot}4 \pm 0{\cdot}1$]. Good agreement between *calculated* changes in CMR_{O_2} based on BOLD theory and the independently *measured* changes in CMR_{O_2} based on ^{13}C-MRS (see Appendix A) demonstrates the quality of the BOLD calibration. (Adapted from Hyder *et al*. 2001.)

(C 2) and (C 3). The value of $T^*_{2,\mathrm{tissue}}$ is much smaller than $T_{2,\mathrm{tissue}}$, and both become progressively smaller at higher B_0 (Kennan *et al*. 1994).

Since $\Delta S/S$ depends upon the balance between delivery of oxygenated blood by perfusion (i.e. CBF) and the rate of oxygen use (i.e. CMR_{O_2}) at steady state, it can be expressed by changes in neurophysiological parameters based on Fick's principle (Ogawa *et al*. 1993)

$$\Delta S/S = \acute{A}((\Delta\mathrm{CBF}/\mathrm{CBF} - \Delta CMR_{O_2}/CMR_{O_2})/(1 + \Delta\mathrm{CBF}/\mathrm{CBF}) - \Delta\mathrm{CBV}/\mathrm{CBV}), \qquad \text{(C 4)}$$

where $\acute{A}$ is a measurable physiological and B_0-dependent constant (given by the product of $1/T_{2,\mathrm{tissue}} \times TE$) and $\Delta CMR_{O_2}/CMR_{O_2}$, $\Delta\mathrm{CBF}/\mathrm{CBF}$, and $\Delta\mathrm{CBV}/\mathrm{CBV}$ are the changes in oxygen consumption, blood flow, and blood volume, respectively (Hyder *et al*. 1998, 2001). Different BOLD calibration methods (e.g. Davis *et al*. 1998; van Zijl *et al*. 1998; Hoge *et al*. 1999; Kim *et al*. 1999; Mandeville *et al*. 1999) have been used to derive quantitative changes in CMR_{O_2} from Eq. (C 4). Some of these methods require additional assumptions, e.g. a hypercapnic challenge which is assumed to induce *only* a hemodynamic response so that the value of $\acute{A}$ determined from such a calibration may underestimate the changes in oxygen consumption.

The different parameters in Eq. (C 4), which model the BOLD signal, have been measured independently in the rat brain cortex. We have made multi-modal MRI and MRS measurements of changes in CMR_{O_2}, CBF, CBV, and the BOLD signal in rat brain (Kida *et al*. 1999, 2000; Hyder *et al*. 2001). Each parameter in Eq. (C 4) is measured independently over a wide range of activity. The calculated changes in CMR_{O_2} based on Eq. (C 4) have been compared with independently *measured* changes in CMR_{O_2} from *in vivo* ^{13}C-MRS detection of ^{13}C label flow from glucose to glutamate under the same conditions (Fig. 14). This agreement has validated deriving $\Delta CMR_{O_2}/CMR_{O_2}$ quantitatively from the BOLD signal.

https://doi.org/10.1017/S0033583502003803 Published online by Cambridge University Press

16. Appendix D. Comparison of spiking activity of a neuronal ensemble with CMR_{O_2}

Experiments comparing stimulation-induced changes in spiking frequency ($\Delta\nu\,\%$) of a neuronal ensemble with changes in energy consumption ($\Delta CMR_{O_2}\,\%$) derived from BOLD experiments were made in rats at two different depths (light and deep) of α-chloralose anesthesia (Smith *et al*. 2002). In each baseline condition the same forepaw stimulation was applied, resulting in a total of four activity levels (i.e. two baseline and two stimulated conditions).

Values of $\Delta\nu\,\%$ were determined from extracellular recordings with microelectrodes and compared with values of $\Delta CMR_{O_2}\,\%$ from calibrated BOLD of the same voxels. Several spiking neurons (predominantly pyramidal cells) were measured in each rat. To adequately represent the activity of a neuronal population in the fMRI-defined region of the cortex, measurements were repeated multiple times. The skull above an activated BOLD focus was thinned and a high impedance tungsten–iridium microelectrode was inserted to the depth of cortical layer 4. The raw extracellular signals were bandpass-filtered and amplified prior to digitization. High signal-to-noise ratio action potentials were identified off-line (Zouridakis & Tam, 2000) with a commercially available spike recognition program (Spike-2, CED,

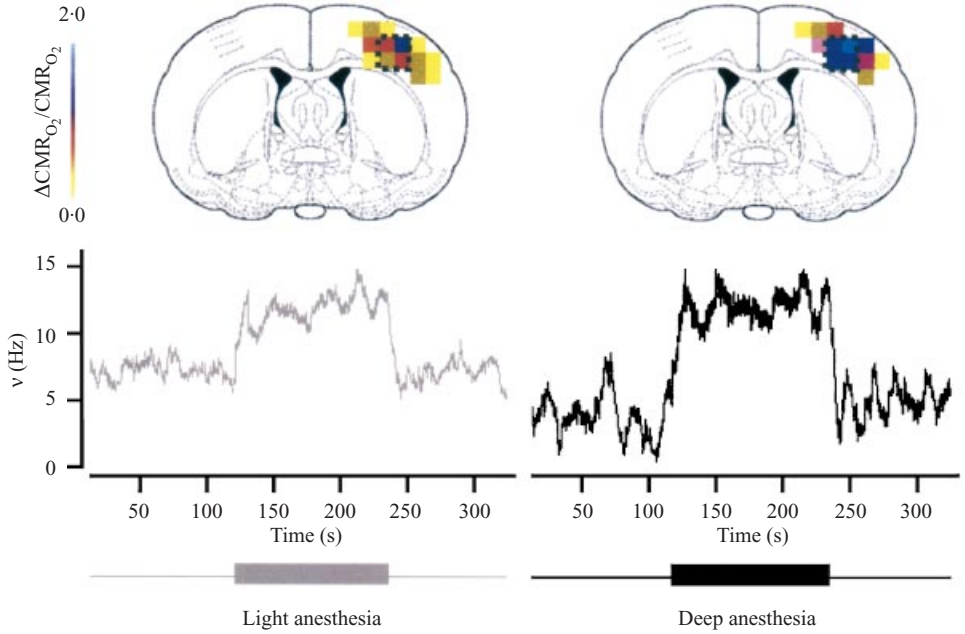


Fig. 15. Localized changes in energy metabolism (ΔCMR_{O_2}) and spiking frequency (ν) of a neuronal ensemble in the contralateral rat cortex during forepaw stimulation. In each case, the fMRI and electrophysiology measurements were made in each rat first under high basal activity (light anesthesia) then under low basal activity (deep anesthesia), using two different doses of α-chloralose. The $\Delta CMR_{O_2}/CMR_{O_2}$ maps (overlaid on stereotaxic coordinates from Paxinos & Watson, 1997) were determined from calibrated BOLD (Hyder *et al*. 2001), whereas the $\Delta\nu/\nu$ values were extracted from extracellular recordings (Smith *et al*. 2002). Approximately 92% of all microelectrode penetrations (in layer 4) identified at least two discrete neurons from the spike analysis (see Fig. 16). No significant stimulation-induced changes in ν and CMR_{O_2} were observed in the ipsilateral side (data not shown).

https://doi.org/10.1017/S0033583502003803 Published online by Cambridge University Press

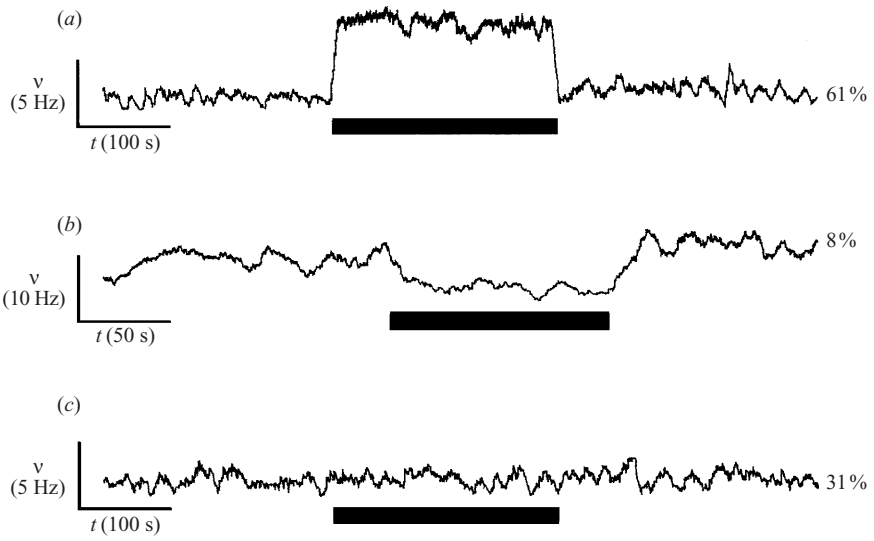


Fig. 16. Experimental variations across electrophysiological measurements (shown for deep anesthesia level only) from the contralateral forepaw region. Significant increases and decreases in ν were observed in 61 and 8% of the recordings, respectively [(*a*) and (*b*), respectively], whereas in 31% of the recordings the stimulation did not induce any significant changes in ν (*c*). The vertical and horizontal bars represent the scales for ν and time, respectively. The thick black horizontal bar represents the duration of the stimulus. (Adapted from Smith *et al.* 2002.)

Cambridge, UK). The temporal history of the population was then followed through for all four conditions (per rat). The spiking data were converted to reflect the relative spiking frequency of the neuronal ensemble by analyzing consecutive 10-s bins.

Figure 15 shows the localized changes in CMR_{O_2} and ν from the contralateral rat cortex during forepaw stimulation. In the same rat, the same stimulation induced different increments in CMR_{O_2} for light and deep anesthesia (by $\sim 40\%$ and $\sim 100\%$), and CMR_{O_2} differed between the two baseline conditions (by $\sim 30\%$). Similar anesthetic dose-dependence decrease of energy metabolism between baseline conditions has been observed with halothane (Savaki *et al.* 1981), α-chloralose (Dudley *et al.* 1982), and phenobarbital (Hodes *et al.* 1985). The stimulation increased averaged contralateral values of ν by $\sim 30\%$ and $\sim 100\%$ for light and deep anesthesia in the same rat, in agreement with the changes in CMR_{O_2}. Baseline-dependent stimulation-induced increments in neuronal activity have been observed under anesthesia (Harding *et al.* 1979; Bonvento *et al.* 1994; Shulman *et al.* 1999). The incremental changes in both CMR_{O_2} and ν were greater from deep anesthesia than from light anesthesia where the baseline was lower by $\sim 30\%$.

Since more than 90% of all microelectrode penetrations yielded at least two discrete and recognizable neurons, multiple electrode measurements provided a reasonable activity estimate of the entire neuronal ensemble ($n = 72$). In the main text, the histograms of ν for all four conditions studied (Fig. 8) show that during stimulation the distributions of ν became similar. Statistically significant increases and decreases in ν were observed upon stimulation in $\sim 60\%$ and $\sim 10\%$ of the recordings, respectively, whereas there were no statistically significant changes in $\sim 30\%$ of the recordings (Fig. 16). Similar behaviors of neuronal ensembles in the cerebral cortex have been reported previously (McCasland & Woolsey, 1988; Scannell & Young, 1999).

https://doi.org/10.1017/S0033583502003803 Published online by Cambridge University Press

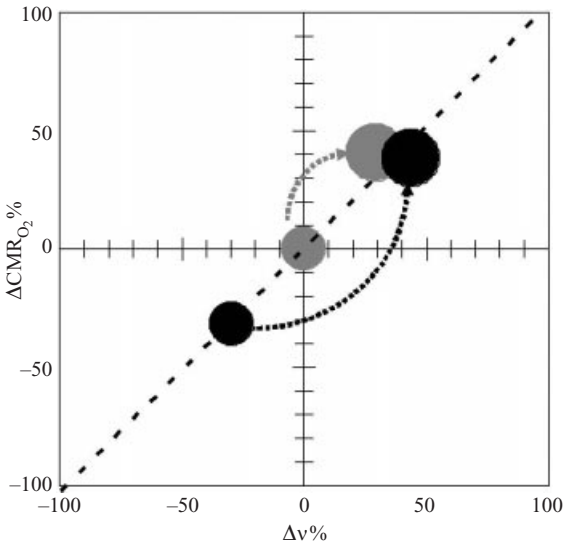


Fig. 17. Relationship between ΔCMR_{O_2}% and $\Delta\nu$% in α-chloralose-anesthetized rats. The sizes of circles represent the mean $\pm$ the largest standard deviation from all rats studied. The data from light and deep anesthesia levels are shown in gray and black, respectively, where the arrows show the increment upon stimulation from the respective baseline levels. The final level reached upon stimulation from both 'baseline' conditions are similar within experimental errors. The dotted line represents the best linear regression ($R^2 = 0{\cdot}98$) of the pooled data. The overall changes in CMR_{O_2} and ν from all rats studied are plotted to show a relationship of $\sim 1{:}1$ between ΔCMR_{O_2}% and $\Delta\nu$%. (Adapted from Smith *et al*. 2002.)

Figure 17 shows that the fractional changes in CMR_{O_2} were ~ 40 % and ~ 100 % from the respective baseline levels, whereas the changes in ν were ~ 30 % and ~ 100 %. The changes in CMR_{O_2} and ν upon forepaw stimulation were greater for deep anesthesia which, when added to its lowered baseline values, brought each parameter to approximately the same absolute value during stimulation. The current results show that $\Delta CMR_{O_2}\% \approx \Delta\nu\%$ [see Eq. (2)]. Furthermore, the increments of CMR_{O_2} and ν upon forepaw stimulation elevated each signal to the same final values in both conditions (Fig. 7), in agreement with a previous hypothesis (Shulman *et al*. 1999). The data shown in Fig. 17 were normalized to the non-stimulated baseline condition of light anesthesia. These results are consistent with observation in peripheral neurons (Sokoloff, 1993) where glucose metabolism increased proportionately with the stimulation frequency.

17. References

Anderson, C. M. & Swanson, R. A. (2000). Astrocyte glutamate transport: review of properties, regulation, and physiological functions. *Glia* **32**, 1–14.

Attwell, D. & Laughlin, S. B. (2001). An energy budget for signaling in the grey matter of the brain. *J. cereb. Blood Flow Metab.* **21**, 1133–1145.

Badar-Goffer, R. S., Bachelard, H. S. & Morris, P. G. (1990). Cerebral metabolism of acetate and glucose studied by ^{13}C-N.M.R. spectroscopy. A technique for investigating metabolic compartmentation in the brain. *Biochem. J.* **266**, 133–139.

Bandettini, P. A., Wong, E. C., Hinks, R. S., Tikofsky, R. S. & Hyde, J. S. (1992). Time course EPI of human brain function during task activation. *Magn. Reson. Med.* **25**, 390–397.

Behar, K. L., Petroff, O. A. C., Prichard, J. W., Alger, J. R. & Shulman, R. G. (1986). Detection of metabolites in rabbit brain by ^{13}C NMR spectroscopy following administration of [1-^{13}C]glucose. *Magn. Reson. Med.* **3**, 911–920.

https://doi.org/10.1017/S0033583502003803 Published online by Cambridge University Press

Berl, S., Nicklas, W. J. & Clarke, D. D. (1970). Compartmentation of citric acid cycle metabolism in brain, labelling of glutamate, glutamine, aspartate and GABA by several radioactive tracer metabolites. *J. Neurochem*. **17**, 1009–1015.

Blamire, A. M., Ogawa, S., Ugurbil, K., Rothman, D., McCarthy, G., Ellermann, J. M., Hyder, F., Rattner, Z. & Shulman, R. G. (1992). Dynamic mapping of the human visual cortex by high-speed magnetic resonance imaging. *Proc. natn. Acad. Sci. USA* **89**, 11069–11073.

Bonvento, G., Charbonne, R., Correze, J. L., Borredon, J., Seylaz, J. & Lacombe, P. (1994). Is alpha-chloralose plus halothane induction a suitable anesthetic regimen for cerebrovascular research? *Brain Res*. **665**, 213–221.

Braitenberg, V. & Schuz, A. (1991). *Anatomy of the Cortex: Statistics and Geometry*. Berlin: Springer.

Brinker, G., Bock, C., Busch, E., Krep, H., Hossmann, K. A. & Hoehn-Berlage, M. (1999). Simultaneous recording of evoked potentials and T_2*-weighted MR images during somatosensory stimulation of rat. *Magn. Reson. Med*. **41**, 469–473.

Bush, G., Vogt, B. A., Holmes, J., Dale, A. M., Greve, D., Jenike, M. A. & Rosen, B. R. (2002). Dorsal anterior cingulate cortex: a role in reward-based decision making. *Proc. natn. Acad. Sci. USA* **99**, 523–528.

Calamante, F., Thomas, D. L., Pell, G. S., Wiersma, J. & Turner, R. (1999). Measuring cerebral blood flow using magnetic resonance imaging techniques. *J. cereb. Blood Flow Metab*. **19**, 701–735.

Cerdan, S., Kunnecke, B. & Seelig, J. (1990). Cerebral metabolism of [1,2-^{13}C] acetate as detected by in vivo and in vitro ^{13}C NMR. *J. biol. Chem*. **265**, 12916–12926.

Changeux, J. P. (1985). *Neuronal Man: The Biology of Mind* (translated by L. Garcy). Princeton, NJ: Princeton University Press.

Chapin, J. K. & Nicolelis, M. A. (1999). Principal component analysis of neuronal ensemble activity reveals multidimensional somatosensory representations. *J. Neurosci. Methods* **94**, 121–140.

Davis, T. L., Kwong, K. K., Weisskoff, R. M. & Rosen, B. R. (1998). Calibrated functional MRI: mapping the dynamics of oxidative metabolism. *Proc. natn. Acad. Sci. USA* **95**, 1834–1839.

Dehaene, S., Kerszberg, M. & Changeux, J. P. (1998). A neuronal model of a global workspace in effortful cognitive tasks. *Proc. natn. Acad. Sci. USA* **95**, 14529–14534.

des Rosiers, M. H., Sakurada, O., Jehle, J., Shinohara, M., Kennedy, C. & Sokoloff, L. (1978). Functional plasticity in the immature striate cortex of the monkey shown by the [^{14}C]deoxyglucose method. *Science* **200**, 447–449.

Desimone, R. (1996). Neural mechanisms for visual memory and their role in attention. *Proc. natn. Acad. Sci. USA* **93**, 13494–13499.

Dietrich, W. D., Ginsberg, M. D. & Busto, R. (1986). Effect of transient cerebral ischemia on metabolic activation of a somatosensory circuit. *J. cereb. Blood Flow Metab*. **6**, 405–413.

Disbrow, E. A., Slutsky, D. A., Roberts, T. P. & Krubitzer, L. A. (2001). Functional MRI at 1.5 Tesla: a comparison of the blood oxygenation level-dependent signal and electrophysiology. *Proc. natn. Acad. Sci. USA* **97**, 9718–9723.

Dudley, R. E., Nelson, S. R. & Samson, F. (1982). Influence of chloralose on brain regional glucose utilization. *Brain Res*. **233**, 173–180.

Fitzpatrick, S. M., Hetherington, H. P., Behar, K. L. & Shulman, R. G. (1990). The flux from glucose to glutamate in the rat brain in vivo as determined by ^{1}H-observed, ^{13}C-edited NMR spectroscopy. *J. cereb. Blood Flow Metab*. **10**, 170–179.

Fox, P. T. & Raichle, M. E. (1986). Focal physiological uncoupling of cerebral blood flow and oxidative metabolism during somatosensory stimulation in human subjects. *Proc. natn. Acad. Sci. USA* **83**, 1140–1144.

Fox, P. T., Raichle, M. E., Mintun, M. A. & Dence, C. (1988). Nonoxidative glucose consumption during focal physiologic neural activity. *Science* **241**, 462–464.

Frahm, J., Kruger, G., Merboldt, K. D. & Kleinschmidt, A. (1996). Dynamic uncoupling and recoupling of perfusion and oxidative metabolism during focal brain activation in man. *Magn. Reson. Med*. **35**, 143–148.

Georgopoulos, A. P. (2000). Neural aspects of cognitive motor control. *Curr. Opin. Neurobiol*. **10**, 238–241.

Ginsberg, M. D., Dietrich, W. D. & Busto, R. (1987). Coupled forebrain increases of local cerebral glucose utilization and blood flow during physiologic stimulation of a somatosensory pathway in the rat: demonstration by double-label autoradiography. *Neurology* **37**, 11–19.

Gjedde, A. (1997). The relation between brain function and cerebral blood flow and metabolism. In *Cerebrovascular Disease* (ed. H. H. Batjer), pp. 23–40. Philadelphia: Lippincott-Raven.

Goldman-Rakic, P. S. (1996). Regional and cellular fractionation of working memory. *Proc. natn. Acad. Sci. USA* **93**, 13473–13480.

Gray, C. M. (1995). Synchronous oscillations in neuronal systems: mechanisms and functions. *J. Comput. Neurosci*. **1**, 11–38.

Gruetter, R., Novotny, E. J., Boulware, S. D., Mason, G. F., Rothman, D. L., Prichard, J. W. & Shulman, R. G. (1994). Localized ^{13}C NMR spectro-

https://doi.org/10.1017/S0033583502003803 Published online by Cambridge University Press

scopy in the human brain of amino acid labeling from ^{13}C glucose. *J. Neurochem.* **63**, 1377–1385.

Gruetter, R., Seaquist, E. R., Kim, S. & Ugurbil, K. (1998). Localized in vivo ^{13}C-NMR of glutamate metabolism in the human brain: initial results at 4 Tesla. *Dev. Neurosci.* **20**, 380–388.

Gusnard, D. A. & Raichle, M. E. (2001). Searching for a baseline: functional imaging and the resting human brain. *Nat. Rev. Neurosci.* **2**, 685–694.

Harding, G. W., Stogsdill, R. M. & Towe, A. L. (1979). Relative effects of pentobarbital and chloralose on the responsiveness of neurons in sensorimotor cerebral cortex of the domestic cat. *Neuroscience* **4**, 369–378.

Heeger, D. J., Huk, A. C., Geisler, W. & Albrecht, D. G. (2000). Spikes versus BOLD: what does neuroimaging tell us about neuronal activity? *Nat. Neurosci.* **3**, 631–633.

Hoge, R. D., Atkinson, J., Gill, B., Crelier, G. R., Marrett, S. & Pike, G. B. (1999). Linear coupling between cerebral blood flow and oxygen consumption in activated human cortex. *Proc. natn. Acad. Sci. USA* **96**, 9403–9408.

Hyder, F., Chase, J. R., Behar, K. L., Mason, G. F., Siddeek, M., Rothman, D. L. & Shulman, R. G. (1996). Increased tri-carboxylic acid cycle flux in rat brain during forepaw stimulation detected with ^{1}H-[^{13}C] NMR. *Proc. natn. Acad. Sci. USA* **93**, 7612–7617.

Hyder, F., Kennan, R. P., Kida, I., Mason, G. F., Behar, K. L. & Rothman, D. L. (2000). Dependence of oxygen delivery on blood flow in rat brain: a 7 Tesla nuclear magnetic resonance study. *J. cereb. Blood Flow Metab.* **20**, 485–498.

Hyder, F., Kida, I., Behar, K. L., Kennan, R. P., Maciejewski, P. K. & Rothman, D. L. (2001). Quantitative functional imaging of the brain: towards mapping neuronal activity by BOLD fMRI. *NMR Biomed.* **14**, 413–431.

Hyder, F., Renken, R. & Rothman, D. L. (1999). In vivo carbon-edited detection with proton echo-planar spectroscopic imaging (ICED PEPSI): [3,4-$^{13}CH_2$]-glutamate/glutamine tomography in rat brain. *Magn. Reson. Med.* **42**, 997–1003.

Hyder, F., Rothman, D. L., Mason, G. F., Rangarajan, A., Behar, K. L. & Shulman, R. G. (1997). Oxidative glucose metabolism in rat brain during single forepaw stimulation: a spatially localized ^{1}H[^{13}C]NMR study. *J. cereb. Blood Flow Metab.* **17**, 1040–1047.

Hyder, F., Rothman, D. L. & Shulman, R. G. (2002). Total neurenergetics support localized brain activity: implications for the interpretation of fMRI. *Proc. natn. Acad. Sci. USA.* **99**, 10771–10776.

Hyder, F., Shulman, R. G. & Rothman, D. L. (1998). A model for the regulation of cerebral oxygen delivery. *J. Appl. Physiol.* **85**, 554–564.

Kanamori, K. & Ross, B. D. (1993). ^{15}N N.M.R. measurement of the in vivo rate of glutamine synthesis and utilization at steady state in the brain of the hyperammonaemic rat. *Biochem. J.* **293**, 461–468.

Kanamori, K. & Ross, B. D. (1995). In vivo activity of glutaminase in the brain of hyperammonaemic rats measured by ^{15}N nuclear magnetic resonance. *Biochem. J.* **305**, 329–336.

Kandel, E. R., Schwartz, J. H. & Jessell, T. M. (1991). *Principles of Neural Science*. Norwalk, CT: Appleton & Lange.

Kennan, R. P., Scanley, B. E. & Gore, J. C. (1997). Physiologic basis for BOLD MR signal changes due to hypoxia/hyperoxia: separation of blood volume and magnetic susceptibility effects. *Magn. Reson. Med.* **37**, 953–956.

Kennan, R. P., Zhong, J. & Gore, J. C. (1994). Intravascular susceptibility contrast mechanisms in tissue. *Magn. Reson. Med.* **31**, 9–21.

Kennedy, C., Des Rosiers, M. H., Sakurada, O., Shinohara, M., Reivich, M., Jehle, J. W. & Sokoloff, L. (1976). Metabolic mapping of the primary visual system of the monkey by means of the autoradiographic [^{14}C]deoxyglucose technique. *Proc. natn. Acad. Sci. USA* **73**, 4230–4234.

Kida, I., Hyder, F. & Behar, K. L. (2001). Inhibition of voltage-dependent sodium channels suppresses the functional MRI response to forepaw somatosensory activation in the rodent. *J. cereb. Blood Flow Metab.* **21**, 585–591.

Kida, I., Hyder, F., Kennan, R. P. & Behar, K. L. (1999). Towards absolute quantitation of BOLD functional MRI. *Adv. exp. med. Biol.* **471**, 681–689.

Kida, I., Kennan, R. P., Rothman, D. L., Behar, K. L. & Hyder, F. (2000). High-resolution CMR_{O_2} mapping in rat cortex: a multi-parametric approach to calibration of BOLD image contrast at 7 Tesla. *J. cereb. Blood Flow Metab.* **20**, 847–860.

Kim, S. G., Rostrup, E., Larsson, H. B., Ogawa, S. & Paulson, O. B. (1999). Determination of relative CMR_{O_2} from CBF and BOLD changes: significant increase of oxygen consumption rate during visual stimulation. *Magn. Reson. Med.* **41**, 1152–1161.

Kossut, M., Hand, P. J., Greenberg, J. & Hand, C. L. (1988). Single vibrissal cortical column in SI cortex of rat and its alterations in neonatal and adult vibrissa-deafferented animals: a quantitative 2DG study. *J. Neurophysiol.* **60**, 829–852.

Kreuzer, F. (1982). Oxygen supply to tissues: the Krogh model and its assumptions. *Experientia* **38**, 1415–1426.

Kristan, Jr., W. B. & Shaw, B. K. (1997). Population coding and behavioral choice. *Curr. Opin. Neurobiol.* **7**, 826–831.

Krogh, A. (1919). The number and the distribution of capillaries in muscles with the calculation of the

https://doi.org/10.1017/S0033583502003803 Published online by Cambridge University Press

oxygen pressure head necessary for supplying the tissue. *J. Physiol.* (*Lond.*) **52**, 409–441.

Kuschinsky, W., Suda, S. & Sokoloff, L. (1981). Local cerebral glucose utilization and blood flow during metabolic acidosis. *Amer. J. Physiol.* **241**, H772–H777.

Kwong, K. K., Belliveau, J. W., Chesler, D. A., Goldberg, I. E., Weiskoff, R. M., Poncelet, B. P., Kennedy, D. N., Hoppel, B. E., Cohen, M. S., Turner, R., Cheng, H. M., Brady, T. J. & Rosen, B. R. (1992). Dynamic magnetic resonance imaging of human brain activity during primary sensory stimulation. *Proc. natn. Acad. Sci. USA* **89**, 5675–5679.

Lebon, V., Petersen, K. F., Cline, G. W., Shen, J., Mason, G. F., Dufour, S., Behar, K. L., Shulman, G. I. & Rothman, D. L. (2002). Astroglial contribution to brain energy metabolism in humans revealed by ^{13}C nuclear magnetic resonance spectroscopy: elucidation of the dominant pathway for neurotransmitter glutamate repletion and measurement of astrocytic oxidativemetabolism. *J. Neurosci.* **22**, 1523–1531.

Logothetis, N. K. (2000). Object recognition: holistic representations in the monkey brain. *Spat. Vis.* **13**, 165–178.

Logothetis, N. K., Pauls, J., Augath, M., Trinath, T. & Oeltermann, A. (2001). Neurophysiological investigation of the basis of the fMRI signal. *Nature* **412**, 150–157.

Magistretti, P. J., Pellerin, L., Rothman, D. L. & Shulman, R. G. (1999). Energy on demand. *Science* **283**, 496–497.

Mandeville, J. B., Marota, J. J., Ayata, C., Moskowitz, M. A., Weisskoff, R. M. & Rosen, B. R. (1999). MRI measurement of the temporal evolution of relative $CMRO_2$ during rat forepaw stimulation. *Magn. Reson. Med.* **42**, 944–951.

Mason, G. F., Gruetter, R., Rothman, D. L., Behar, K. L., Shulman, R. G. & Novotny, E. J. (1995). Simultaneous determination of the rates of the TCA cycle: glucose utilization, α-ketoglutarate/glutamate exchange, and glutamine synthesis in human brain by NMR. *J. cereb. Blood Flow Metab.* **15**, 12–25.

Mason, G. F., Rothman, D. L., Behar, K. L. & Shulman, R. G. (1992). NMR determination of the TCA cycle rate and α-ketoglutarate/glutamate exchange rate in rat brain. *J. cereb. Blood Flow Metab.* **12**, 434–447.

McCasland, J. S. & Woolsey, T. A. (1988). High-resolution 2-deoxyglucose mapping of functional cortical columns in mouse barrel cortex. *J. comp. Neurol.* **278**, 555–569.

Mies, G., Niebuhr, I. & Hossmann, K. A. (1981a). Simultaneous measurement of blood flow and glucose metabolism by autoradiographic techniques. *Stroke* **12**, 581–588.

Mies, G., Niebuhr, I. & Hossmann, K. A. (1981b). A double tracer autoradiographic technique for simultaneous measurement of cerebral blood flow and cerebral metabolism in rats. *Eur. Neurol.* **20**, 188–193.

Mintun, M. A., Raichle, M. E., Martin, W. R. & Herscovitch, P. (1984). Brain oxygen utilization measured with O-15 radiotracers and positron emission tomography *J. Nucl. Med.* **25**, 177–187.

Mintun, M. A., Vlassenko, A. G., Shulman, G. L. & Snyder, A. Z. (2002). Time-related increase of oxygen utilization in continuously activated human visual cortex. *Neuroimage* **16**, 531–537.

Ogawa, S., Lee, T. M., Nayak, A. S. & Glynn, P. (1990). Oxygenation-sensitive contrast in magnetic resonance image on rodent brain at high magnetic fields. *Magn. Reson. Med.* **14**, 68–78.

Ogawa, S., Lee, T. M., Stepnoski, R., Chen, W., Zhu, X. H. & Ugurbil, K. (2000). An approach to probe some neural systems interaction by functional MRI at neural time scale down to milliseconds. *Proc. natn. Acad. Sci. USA* **97**, 11026–11031.

Ogawa, S., Menon, R. S., Kim, S. G. & Ugurbil, K. (1998). On the characteristics of functional magnetic resonance imaging of the brain. *Annu. Rev. Biophys. biomol. Struct.* **27**, 447–474.

Ogawa, S., Menon, R. S., Tank, D. W., Kim, S. G., Merkle, H., Ellermann, J. M. & Ugurbil, K. (1993). Functional brain mapping by blood oxygenation level-dependent contrast magnetic resonance imaging. *Biophys. J.* **64**, 803–812.

Ogawa, S., Tank, D. W., Menon, R., Ellermann, J. M., Kim, S. G., Merkle, H. & Ugurbil, K. (1992). Intrinsic signal changes accompanying sensory stimulation: functional brain mapping with magnetic resonance imaging. *Proc. natn. Acad. Sci. USA* **89**, 5951–5955.

Paxinos, G. & Watson, C. (1997). *The Rat Brain in Stereotaxic Coordinates*. New York: Academic Press.

Pellerin, L. & Magistretti, P. J. (1994). Glutamate uptake into astrocytes stimulates aerobic glycolysis: a mechanism coupling neuronal activity to glucose utilization. *Proc. natn. Acad. Sci. USA* **91**, 10625–10629.

Peng, L., Hertz, L., Huang, R., Sonnewald, U., Petersen, S. B., Westergaard, N., Larsson, O. & Schousboe, A. (1993). Utilization of glutamine and of TCA cycle constituents as precursors for transmitter glutamate and GABA. *Dev. Neurosci.* **15**, 367–377.

Phelps, M. E., Huang, S. C., Hoffman, E. J., Selin, C., Sokoloff, L. & Kuhl, D. E. (1979). Tomographic measurement of local cerebral glucose metabolic rate in humans with [^{18}F]2-fluoro-2-deoxy-D-glucose: validation of method. *Ann. Neurol.* **6**, 371–388.

Posner, M. I. & Raichle, M. E. (1998). The neuroimaging of human brain function. *Proc. natn. Acad. Sci. USA* **95**, 763–764.

https://doi.org/10.1017/S0033583502003803 Published online by Cambridge University Press

Prichard, J. W., Petroff, O. A. C., Ogino, T. & Shulman, R. G. (1987). Cerebral lactate elevation by electroshock: a ^{1}H magnetic resonance study. *Ann. NY Acad. Sci.* **508**, 54–63.

Prichrad, J., Rothman, D., Novotny, E., Petroff, O., Kuwabara, T., Avison, M., Howseman, A., Hanstock, C. & Shulman, R. (1991). Lactate rise detected by ^{1}H NMR in human visual cortex during physiologic stimulation. *Proc. natn. Acad. Sci. USA* **88**, 5829–5831.

Raichle, M. E. (1988). Circulatory and metabolic correlates of brain function in normal humans. In *Handbook of Physiology – The Nervous System V*, pp. 633–674. New York: Springer-Verlag.

Raichle, M. E. (1998). Behind the scenes of functional brain imaging: a historical and physiological perspective. *Proc. natn. Acad. Sci. USA* **95**, 765–772.

Raichle, M. E., Martin, W. R., Herschvitch, P., Mintun, M. A. & Markham, J. (1983). Brain blood flow measured with intravenous $H_2{}^{15}O$. II. Implementation and validation. *J. Nucl. Med.* **24**, 790–798.

Raichle, M. E., Welch, M. J., Grubb, Jr., R. L., Larson, K. B., Laux, B. E. & Ter-Pogossian, M. M. (1979). Regional cerebral oxygen utilization with positron emission tomography. *Trans. Amer. Neurol. Assoc.* **104**, 154–156.

Rees, G., Friston, K. & Koch, C. (2000). A direct quantitative relationship between the functional properties of human and macaque V5. *Nat. Neurosci.* **3**, 716–723.

Reivich, M., Kuhl, D., Wolf, A., Greenberg, J., Phelps, M., Ido, T., Casella, V., Fowler, J., Hoffman, E., Alavi, A., Som, P. & Sokoloff, L. (1979). The [^{18}F]fluorodeoxyglucose method for the measurement of local cerebral glucose utilization in man. *Circ. Res.* **44**, 127–137.

Richard, C. D. (1998). What the actions of anaesthetics on fast synaptic transmission reveal about the molecular mechanism of anaesthesia. *Toxicol. Lett.* **100–101**, 41–50.

Rolls, E. T. (2000). Functions of the primate temporal lobe cortical visual areas in invariant visual object and face recognition. *Neuron* **27**, 205–218.

Rothman, D. L., Behar, K. L., Hetherington, H. P., Den Hollander, J. A., Bendall, M. R., Petroff, O. A. C. & Shulman, R. G. (1985). ^{1}H observed ^{13}C decoupled spectroscopic measurements of lactate and glutamate the rat brain in vivo. *Proc. natn. Acad. Sci. USA* **82**, 1633–1637.

Rothman, D. L., Hyder, F., Sibson, N., Behar, K. L., Mason, G. F., Shen, J., Petroff, O. A. C. & Shulman, R. G. (2002). In vivo magnetic resonance spectroscopy studies of the glutamate and GABA neurotransmitter cycles and functional neuroenergetics. In *Neuropsychopharmacology, The Fifth Generation of Progress* (eds. K. L. Davis, D. Charney, J. T. Coyle & C. Nemeroff), pp. 315–342. Philadelphia: Lippincott, Williams & Wilkins.

Rothman, D. L., Sibson, N. R., Hyder, F., Shen, J., Behar, K. L. & Shulman, R. G. (1999). In vivo nuclear magnetic resonance spectroscopy studies of the relationship between the glutamate-glutamine neurotransmitter cycle and functional neuroenergetics. *Phil. Trans. R. Soc. Lond. B* **354**, 1165–1177.

Roy, C. S. & Sherrington, C. S. (1890). On the regulation of the blood supply of the rat brain. *J. Physiol. (Lond.)* **11**, 85–108.

Sakurada, O., Kennedy, C., Jehle, J., Brown, J. D., Carbin, G. L. & Sokoloff, L. (1978). Measurement of cerebral blood flow with iodo[^{14}C]antipyrine. *Amer. J. Physiol.* **234**, H59–H66.

Santori, E. M., Der, T. & Collins, R. C. (1986). Functional metabolic mapping during forelimb movement in rat. II. Stimulation of forelimb muscles. *J. Neurosci.* **6**, 463–474.

Sappey-Marinier, D., Calabrese, G., Fein, G., Hugg, J. W., Biggins, C. & Weiner, M. W. (1992). Effect of photic stimulation on human visual cortex lactate and phosphates using ^{1}H and ^{31}P magnetic resonance spectroscopy. *J. cereb. Blood Flow Metab.* **12**, 584–592.

Savaki, H. E., Desban, M., Glowinski, J. & Besson, M. J. (1981). Local cerebral glucose consumption in the rat. I. Effects of halothane anesthesia. *J. comp. Neurol.* **213**, 36–45.

Scannell, J. W. & Young, M. P. (1999). Neuronal population activity and functional imaging. *Proc. R. Soc. Lond. B, Biol. Sci.* **266**, 875–881.

Shen, J., Petersen, K. F., Behar, K. L., Brown, P., Nixon, T. W., Mason, G. F., Petroff, O. A. C., Shulman, G. I. & Shulman, R. G. (1999). Determination of the rate of the glutamate-glutamine cycle in the human brain by in vivo ^{13}C NMR. *Proc. natn. Acad. Sci. USA* **96**, 8235–8240.

Shen, J., Sibson, N. R., Cline, G., Behar, K. L., Rothman, D. L. & Shulman, R. G. (1998). ^{15}N NMR spectroscopy studies of ammonia transport and glutamine synthesis in the hyperammonemic rat brain. *Dev. Neurosci.* **20**, 438–443.

Shepherd, G. M. (1994). *The Synaptic Organization of the Brain*. New York: Oxford University Press.

Shulman, R. G., Blamire, A. M., Rothman, D. L. & McCarthy, G. (1993). Nuclear magnetic resonance imaging and spectroscopy of human brain function. *Proc. natn. Acad. Sci. USA* **90**, 3127–3133.

Shulman, R. G., Hyder, F. & Rothman, D. L. (2001a). Lactate efflux and the neuroenergetic basis of brain function. *NMR Biomed.* **14**, 389–396.

Shulman, R. G., Hyder, F. & Rothman, D. L. (2001b). Cerebral energetics and the glycogen shunt: neuro-

https://doi.org/10.1017/S0033583502003803 Published online by Cambridge University Press

chemical basis of functional imaging. *Proc. natn. Acad. Sci. USA* **98**, 6417–6422.

Shulman, R. G. & Rothman, D. L. (1998). Interpreting functional imaging studies in terms of neurotransmitter cycling. *Proc. natn. Acad. Sci. USA* **95**, 11993–11998.

Shulman, R. G. & Rothman, D. L. (2001). The 'glycogen shunt' in exercising muscle: a novel role for glycogen in muscle energetics and fatigue. *Proc. natn. Acad. Sci. USA* **98**, 457–461.

Shulman, R. G., Rothman, D. L. & Hyder, F. (1999). Stimulated changes in localized cerebral energy consumption under anesthesia. *Proc. natn. Acad. Sci. USA* **96**, 3245–3250.

Sibson, N. R., Dhankhar, A., Mason, G. F., Behar, K. L., Rothman, D. L. & Shulman, R. G. (1997). In vivo ^{13}C NMR measurements of cerebral glutamine synthesis as evidence for glutamate-glutamine cycling. *Proc. natn. Acad. Sci. USA* **94**, 2699–2704.

Sibson, N. R., Dhankhar, A., Mason, G. F., Rothman, D. L., Behar, K. L. & Shulman, R. G. (1998). Stoichiometric coupling of brain glucose metabolism and glutamatergic neuronal activity. *Proc. natn. Acad. Sci. USA* **95**, 316–321.

Sibson, N. R., Mason, G. F., Shen, J., Cline, G. W., Herskovits, A. Z., Wall, J. E., Behar, K. L., Rothman, D. L. & Shulman, R. G. (2001). In vivo ^{13}C NMR measurement of neurotransmitter glutamate cycling, anaplerosis and TCA cycle flux in rat brain during [2-^{13}C]glucose infusion. *J. Neurochem.* **76**, 975–989.

Siesjo, B. K. (1978). *Brain Energy Metabolism*. New York: Wiley.

Singer, W. (1994). Coherence as an organizing principle of cortical functions. *Int. Rev. Neurobiol.* **37**, 153–83; discussion 203–207.

Smith, A. J., Blumenfeld, H., Behar, K. L., Rothman, D. L., Shulman, R. G. & Hyder, F. (2002). Cerebral energetics and spiking frequency: the neurophysiological basis of fMRI. *Proc. natn. Acad. Sci. USA.* **99**, 10765–10770.

Sokoloff, L. (1981). Relationships among local functional activity, energy metabolism, and blood flow in the central nervous system. *Fedn. Proc.* **40**, 2311–2316.

Sokoloff, L. (1991). Relationship between functional activity and energy metabolism in the nervous system: whether, where and why? In *Brain Work and Mental Activity* (eds. N. A. Lassen, D. H. Ingvar, M. E. Raichle & L. Friberg), pp. 52–64. Copenhagen: Munksgaard.

Sokoloff, L. (1993). Sites and mechanisms of function-related changes in energy metabolism in the nervous system. *Dev. Neurosci.* **15**, 194–206.

Sokoloff, L. (1999). Energetics of functional activation in neural tissues. *Neurochem. Res.* **24**, 321–329.

Sokoloff, L., Reivich, M., Kennedy, C., Des Rosiers, M. H., Patlak, C. S., Pettigrew, K. D., Sakurada, O. & Shinohara, M. (1977). The [^{14}C]deoxyglucose method for the measurement of local cerebral glucose utilization, theory, procedure, and normal values in the conscious and anesthetized albino rat. *J. Neurochem.* **28**, 897–916.

Tanaka, K. (1996). Inferotemporal cortex and object vision. *Annu. Rev. Neurosci.* **19**, 109–139.

Tolias, A. S., Smirnakis, S. M., Augath, M. A., Trinath, T. & Logothetis, N. K. (2002). Motion processing in the macaque, revisited with functional magnetic resonance imaging. *J. Neurosci.* **21**, 8594–8601.

Torgner, I. & Kvamme, E. (1990). Synthesis of transmitter glutamate and the glial-neuron interrelationship. *Molec. chem. Neuropathol.* **12**, 11–17.

Tsacopoulos, M. & Magistretti, P. J. (1996). Metabolic coupling between glia and neurons. *J. Neurosci.* **16**, 877–885.

Tsodyks, M., Kenet, T., Grinvald, A. & Arieli, A. (1999). Linking spontaneous activity of single cortical neurons and the underlying functional architecture. *Science* **286**, 1943–1946.

Ueki, M., Linn, F. & Hossman, K. A. (1988). Functional activation of cerebral blood flow and metabolism and after global ischemia of rat brain. *J. cereb. Blood Flow Metab.* **8**, 486–494.

Ueki, M., Mies, G. & Hossmann, K. A. (1992). Effect of α-chloralose, halothane, pentobarbital and nitrous oxide anesthesia on metabolic coupling in somatosensory cortex of rat. *Acta Anaesthesiol. Scand.* **36**, 318–322.

Ugurbil, K., Adriany, G., Andersen, P., Wei, C., Gruetter, R., Hu, X., Merkle, H., Kim, D. S., Kim, S. G., Strupp, J., Hong, X. & Ogawa, S. (2000). Magnetic resonance studies of brain function and neurochemistry. *Annu. Rev. biomed. Engng* **2**, 633–660.

van den Berg, C. J. & Garfinkel, D. (1971). A simulation study of brain components. Metabolism of glutamate and related substances in mouse brain. *Biochem. J.* **123**, 211–218.

Yang, X., Hyder, F. & Shulman, R. G. (1997). Functional MRI BOLD signal coincides with electrical activity in the rat whisker barrels. *Magn. Reson. Med.* **38**, 874–877.

Zouridakis, G. & Tam, D. C. (2000). Identification of reliable spike templates in multi-unit extracellular recordings using fuzzy clustering. *Comput. Methods Programs Biomed.* **61**, 91–98.

https://doi.org/10.1017/S0033583502003803 Published online by Cambridge University Press